Spatial Pattern Formation in Development

Philip K. Maini
Wolfson Centre for Mathematical Biology,
Mathematical Institute,
Oxford, UK
maini@maths.ox.ac.uk

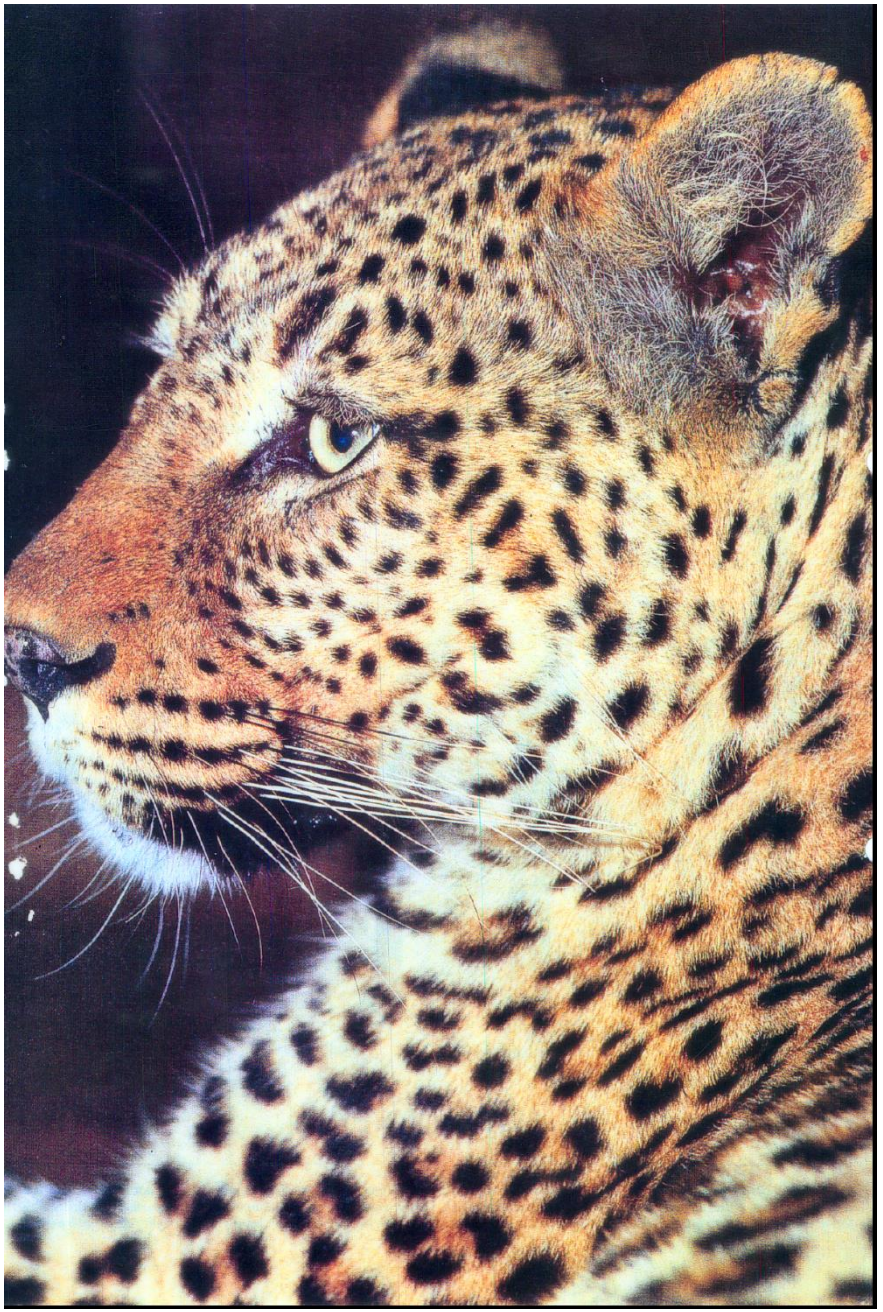

Pattern formation

- How does spatial pattern arise from a fertilised egg which has almost no spatial pattern.

- We see so much spatial pattern – animal coat markings (panda), bones, bacterial patterns, patterns in chemical systems

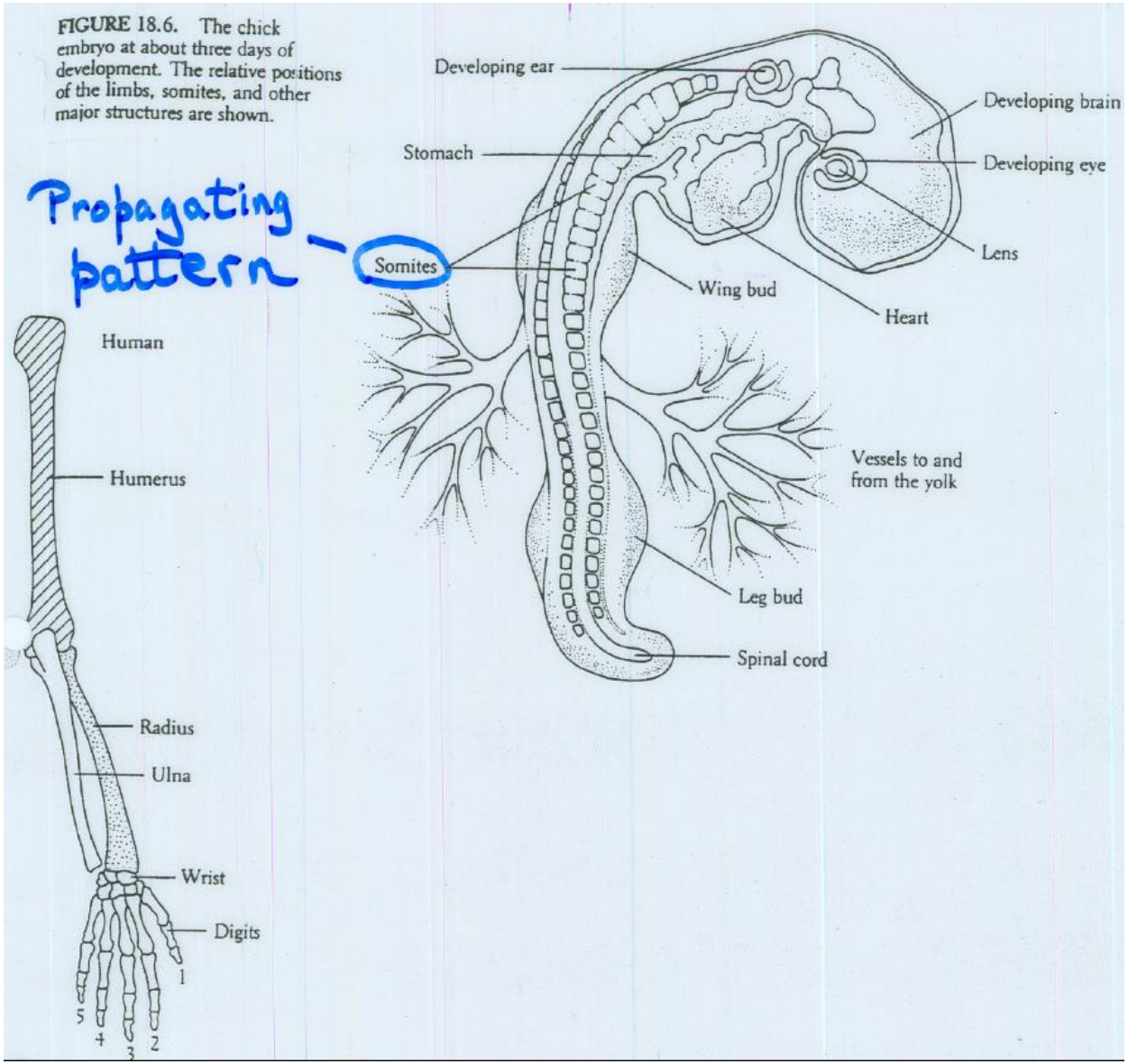

FIGURE 18.6. The chick embryo at about three days of development. The relative positions of the limbs, somites, and other major structures are shown.

Propagating pattern

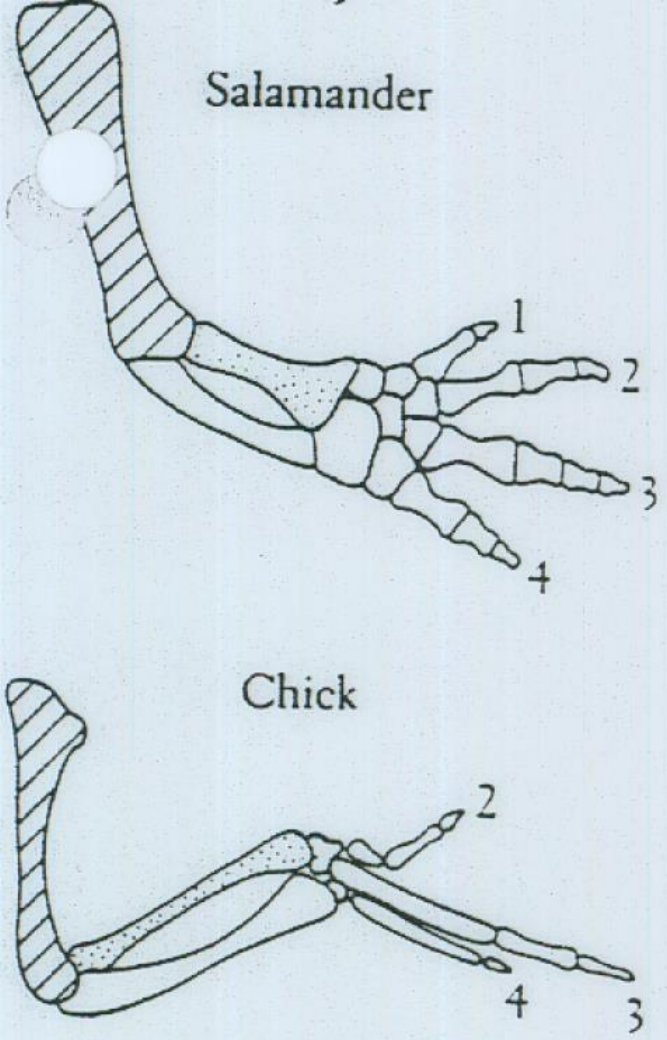

FIGURE 18.2. Drawings of the skeletons of the arm of a human, a salamander, and a chick. The basic pattern is the same in each case, a point emphasized by highlighting comparable bones.

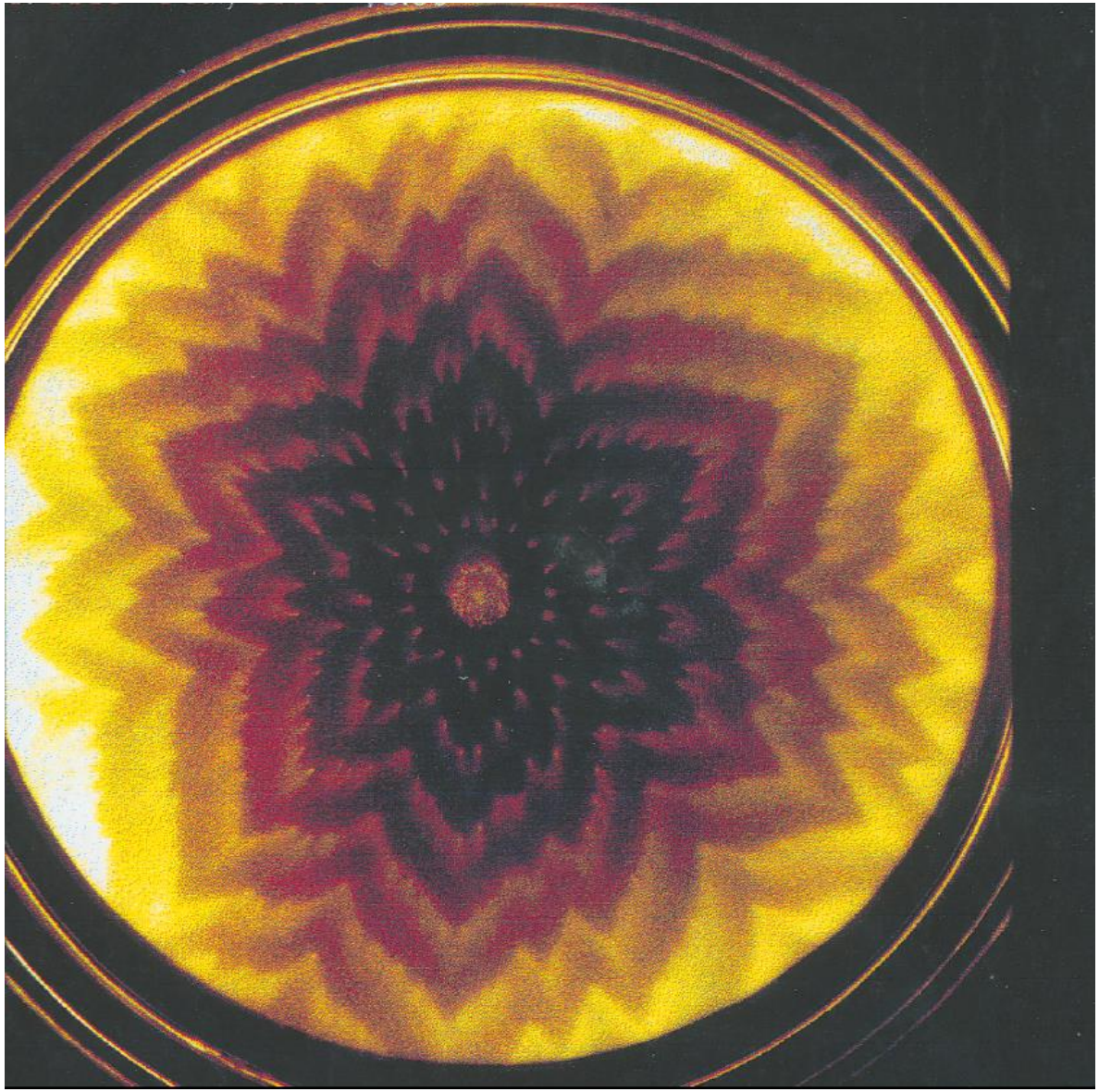

Secrets of self-organization

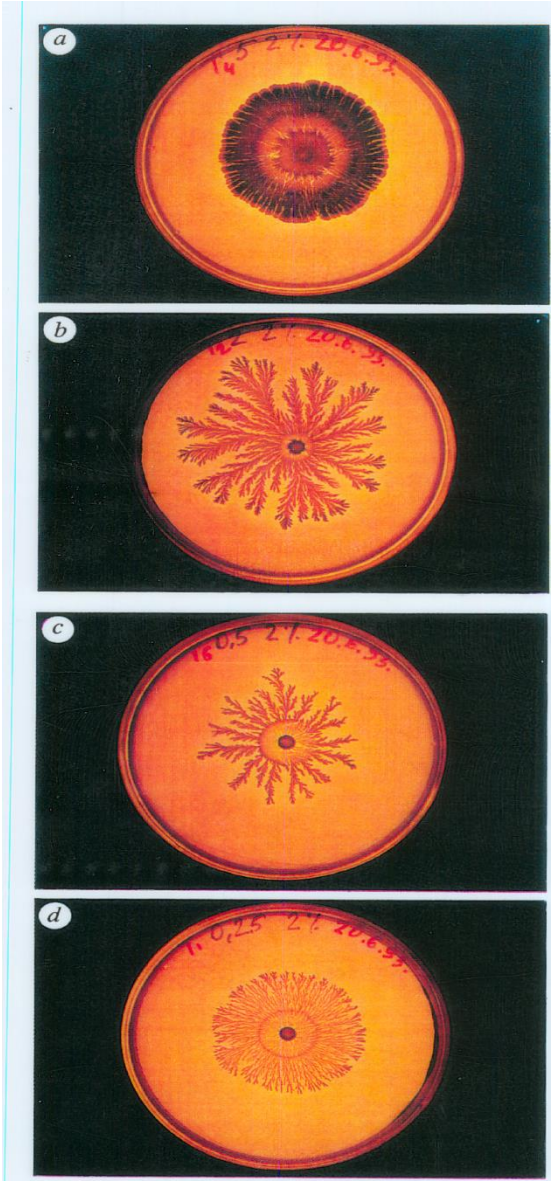
a
b
c
d

How do we explain this?

LECTURE 1: Reaction-diffusion Models

The key idea here is that the flux of material (for example, cells, chemicals, animals) is proportional to the gradient of the flux.

Consider a domain V in R^3, with surface S. Let $c(\underline{x}, t)$ be the concentration of the chemical at position $\underline{x} \in V$. and time t. Assume that the chemical has net production rate $f(c)$.

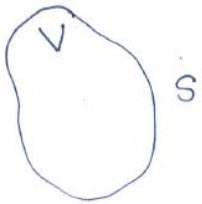

$$\frac{d}{dt}\int_V c(\underline{x},t)\,dv = -\int_S \underline{J}\cdot d\underline{s} + \int_V f\,dv$$

($\underline{J}$: flux)

$$\Rightarrow \int_V \frac{\partial c}{\partial t}\,dv = -\int_V \nabla\cdot\underline{J}\,dv + \int_V f\,dv \qquad \text{(div thm)}$$

$$\Rightarrow \int_V \left(\frac{\partial c}{\partial t} + \nabla\cdot\underline{J} - f\right)dv = 0$$

$$\Rightarrow \frac{\partial c}{\partial t} = f - \nabla\cdot\underline{J} \quad \text{since true } \forall\, V$$

Assume $\underline{J} = -D\nabla c$ (Fick's Law) D = const > 0 = diffusion coefficient

$$\Rightarrow \frac{\partial c}{\partial t} = D\nabla^2 c + f$$

Diffusion is a stabilising process

Let $x \in [0, L]$

$$\frac{\partial c}{\partial t} = D\frac{\partial^2 c}{\partial x^2} + f(c) \qquad -(1)$$

Assume $\exists\ c^* > 0$ such that

$$f(c^*) = 0.$$

Assume boundary conditions:

$$c = c^* \text{ at } x = 0, L \quad \forall t.$$

Linear Stability:

Set $c(x,t) = \tilde{c}(x,t) + c^*$

where $\tilde{c}(x,t)$ is small

$$(1) \Rightarrow \quad \frac{\partial \tilde{c}}{\partial t} = D\frac{\partial^2 \tilde{c}}{\partial x^2} + f'(c^*)\tilde{c} + \text{h.o.t.}$$

using Taylor expansion & the fact that $f(c^*) = 0$.

Using separation of variables, and the fact that $\tilde{c}(x,t) = 0$ at $x = 0, L$

$$\Rightarrow \tilde{c}(x,t) = \sum_{n=1}^{\infty} e^{\left[f'(c^*) - D\left(\frac{n\pi}{L}\right)^2\right]t} \sin\frac{n\pi x}{L}$$

Assume that the steady state is unstable when $D = 0$. Hence $f'(c^*) > 0$.

Then, if $D > \left(\frac{L}{\pi}\right)^2 f'(c^*)$,

c^* is a linearly stable steady state.

$\therefore$ Diffusion is stabilising

Diffusion wipes out pattern

Diffusion

ALAN TURING (1952)

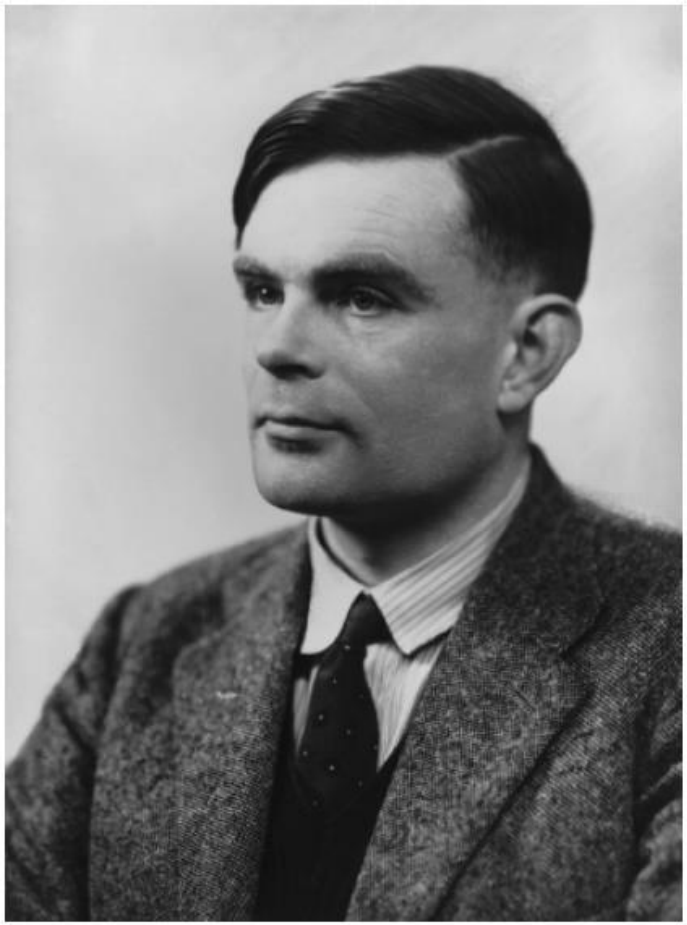

Turing wanted to know how patterns form where, by patterns, he meant, for example, how animals had such colourful *coat markings*, how a *tree branched* (so that it's cross-sectional circular **symmetry was broken**). He concluded that there must be *chemicals* present, to which cells respond, and then there is an *instability* in the chemical pattern that leads to pattern formation.

Symmetry Breaking

For example, in the case of the tree, he assumed that trees respond to a growth hormone that has a circular distribution but that an instability arises that causes it to have local maxima, and this is where the branches form. In general, he called these chemicals "**morphogens**" as they gave rise to form. That is, they form a **pre-pattern** to which cells respond.

The Chemical Basis of Morphogenesis

A. M. Turing

Phil. Trans. R. Soc. Lond. B 1952 **237**, 37-72
doi: 10.1098/rstb.1952.0012

It is suggested that a system of chemical substances, called morphogens, reacting together and diffusing through a tissue, is adequate to account for the main phenomena of morphogenesis.

Diffusion-Driven-Instability

Turing proposed that the patterns that arose via instability were driven **by diffusion!!**

Consider a 2-component System

$$\left.\begin{aligned} \frac{\partial u}{\partial t} &= D_1 \nabla^2 u + f(u,v) \\ \frac{\partial v}{\partial t} &= D_2 \nabla^2 v + g(u,v) \end{aligned}\right\} \quad \begin{aligned} &\underline{x} \in \Omega \subset \mathbb{R}^n \\ &t \in [0,\infty) \end{aligned}$$

initial cond^{ns}: $u(\underline{x},0) = u_0(x)$
$v(\underline{x},0) = v_0(x)$

boundary cond^{ns}: $(\underline{n}.\nabla)u = (\underline{n}.\nabla)v = 0$ on ∂V [zero flux] $\underline{n}$ is outward normal.

Let $\underline{u} = \begin{pmatrix} u \\ v \end{pmatrix}$ $\therefore$ we can rewrite the system as:

$$\underline{u}_t = \underline{F}(\underline{u}) + \underline{\underline{D}}\,\nabla^2 \underline{u} \qquad \frac{\partial u}{\partial n} = 0 \text{ on } \partial\Omega \qquad (2)$$

where $\underline{F}(\underline{u}) = \begin{pmatrix} f(u,v) \\ g(u,v) \end{pmatrix}$, $\underline{\underline{D}} = \begin{bmatrix} D_1 & 0 \\ 0 & D_2 \end{bmatrix}$

Defn. Diffusion-driven instability (Turing instability) occurs when a steady state, stable in the absence of diffusion, goes unstable when diffusion is present.

Let $\underline{u}^*$ be such that $\underline{F}(\underline{u}^*) = \underline{0}$ ($\underline{u}^*$ is const.)

Consider $\underline{w} = \underline{u} - \underline{u}^*$, $\|\underline{w}\| \ll 1$.

Linearising (2): $\underline{w}_t = \underline{F}(\underline{u}^*) + \underline{\underline{M}}\underline{w} + \underline{\underline{D}}\nabla^2\underline{w} + \text{h.o.t.}$

($\underline{F}(\underline{u}^*) \to 0$)

where $\underline{\underline{M}} = \begin{pmatrix} f_u & f_v \\ g_u & g_v \end{pmatrix}_{(u^*, v^*)}$ (Jacobian); $\frac{\partial \underline{w}}{\partial n} = 0$ on $\partial\Omega$

This becomes:

$$\lambda^2 - (\mathrm{tr}\,\underline{\underline{M}} - k^2(D_1+D_2))\lambda + h(k^2) = 0 \qquad (3)$$

where $h(k^2) = D_1 D_2 k^4 - (D_2 f_u + D_1 g_v) k^2 + \det \underline{\underline{M}}$

$\mathrm{Re}\,\lambda < 0 \quad \forall k^2 \Rightarrow \underline{u}^*$ is stable

$\mathrm{Re}\,\lambda > 0$ for some $k^2 \Rightarrow \underline{u}^*$ is unstable.

By the defn of Diffusion-Driven Instability (DDI), the steady state $\underline{u}^*$ must be stable, that is:

$\mathrm{Re}\,\lambda(0) < 0$ i.e. $\lambda^2(0) - (f_u + g_v)\lambda(0) + f_u g_v - f_v g_u = 0$

[eqn (3) with $k^2 = 0$]

must have roots with negative real part.

$$\Rightarrow \quad f_u + g_v < 0 \qquad (C.1)$$

$$f_u g_v - f_v g_u > 0 \qquad (C.2)$$

Now, introduce diffusion, & we require $\mathrm{Re}\,\lambda(k^2) > 0$ for some k^2 in (3).

Ex. Show that this will only occur iff $h(k^2) < 0$ in (3).

The critical (bifurcation) case is:

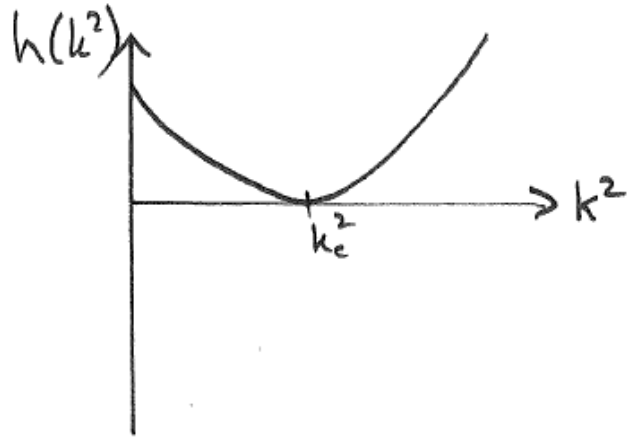

$$D_1 D_2 k_c^4 - (D_2 f_u + D_1 g_v) k_c^2 + f_u g_v - f_v g_u = 0$$

$$\Rightarrow \quad D_2 f_u + D_1 g_v > 0 \qquad (C.3)$$

$$D_2 f_u + D_1 g_v > 2\sqrt{D_1 D_2 (f_u g_v - f_v g_u)} \qquad (C.4)$$

Summary

$$f_u + g_v < 0 \qquad (C.1)$$

$$f_u g_v - f_v g_u > 0 \qquad (C.2)$$

$$D_2 f_u + D_1 g_v > 0 \qquad (C.3)$$

$$D_2 f_u + D_1 g_v > 2\sqrt{D_1 D_2 (f_u g_v - f_v g_u)} \qquad (C.4)$$

Remark 1 $D_1 \neq D_2$

Remark 2 $\underline{\underline{M}}$ can only have sign structure

$$\begin{bmatrix} + & - \\ + & - \end{bmatrix} \quad (a) \qquad \begin{bmatrix} + & + \\ - & - \end{bmatrix} \quad (b)$$

(a) In this case: u activates itself & also activates v
v inhibits u

Also, from (C.1) & (C.3), $D_1 > D_2$

∴ we have <u>short-range activation, long-range inhibition</u>

Consider the case: $x \in [0, L]$ with zero flux boundary conditions.

In this case, $\underline{w} = \sum_{n=0}^{\infty} \underline{\alpha}_n e^{\lambda(k^2)t} \cos\frac{n\pi}{L} x$

where $k^2 = \frac{n^2\pi^2}{L^2}$. $\cos\frac{n\pi x}{L}$ are called <u>admissible modes</u>.

i.e., even though in our analysis $k \in \mathbb{R}$, now we realise for this case that k takes discrete values.

Under (C1)-(C4) $\mathrm{Re}\,\lambda(k^2)$

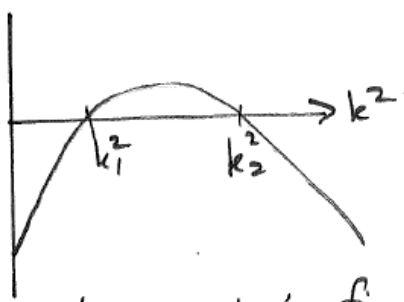

k_1, k_2 are functions of the parameters and $\therefore$ fixed.

- If L is very small, such that $\left.\frac{n^2\pi^2}{L^2}\right|_{n=1} > k_2^2$, then

  $\mathrm{Re}\,\lambda(k^2) < 0 \quad \forall$ admissible modes.

  $\therefore$ no instability.

- As L increases, $k_1^2 < \frac{n^2\pi^2}{L^2} < k_2^2$ holds for increasingly larger n.

  Hence the modes that are selected and grow ($\cos\frac{n\pi x}{L}$) do so for larger n.

- In 2 spatial dimensions, $\underline{x} \in [0,a] \times [0,b]$, $a, b > 0$

& zero flux body cond^{ns}:

$$\underline{\omega} = \sum_{n=0}^{\infty} \sum_{m=0}^{\infty} \underline{\alpha}_{nm} \cos \frac{n\pi x}{a} \cos \frac{m\pi y}{b}$$

and $k^2 = \left(\frac{n^2}{a^2} + \frac{m^2}{b^2} \right) \pi^2$

$\therefore$ if the domain is long and thin ($b \ll 1$) then $m = 0$ for $k_{n,m}^2 \in (k_1^2, k_2^2)$ & we have stripes.

If I have the case such that $k_{n,m}^2 \in (k_1^2, k_2^2)$ for $n = n_0$, $m = m_0$ with n_0, m_0 both non-negative, & I narrow the domain, then $m_0 \to 0$. That is, I transistion from spots to stripes.

[an example of a **DEVELOPMENTAL CONSTRAINT**]

Properties/Predictions

- Minimum domain size for pattern
- Pattern complexity increases with domain size – limb experiments
- Effects of geometry – spots and stripes
- Developmental constraints

Examples of f & g

Gierer-Meinhardt 1972
(phenomenological model)

$$f = k_1 - k_2 u + k_3 \frac{u^2}{v}$$

$$g = k_4 u^2 - k_5 v$$

$k_1 \ldots k_5$ positive constants.

Thomas Model 1975

$$f = k_1 - k_2 u - H(u,v)$$

$$g = k_3 - k_4 v - H(u,v)$$

$$H(u,v) = \frac{k_5 u v}{k_6 + k_7 u + k_8 u^2}$$

$k_1, \ldots k_8$ positive constants.

empirical model for oxygen (v) and uric acid (u).

Schnakenberg 1979

$$f = k_1 - k_2 u + k_3 u^2 v$$

$$g = k_4 - k_5 u^2 v$$

$k_1 \ldots k_5$ positive constants

[$2A + B \xrightarrow{k_3} 3A \Rightarrow k_3 [A]^2 B$ (Law of Mass Action)]

Patterns

Linear analysis turns out to be a pretty good predictor of patterns.

Turing patterns have been found in Chemistry

In chemistry, the groups of DeKepper and Swinney have shown that Turing patterns exist (CIMA – Chloride-Iodide-Malonic-Acid), and they have been modelled by Lengyel and Epstein.

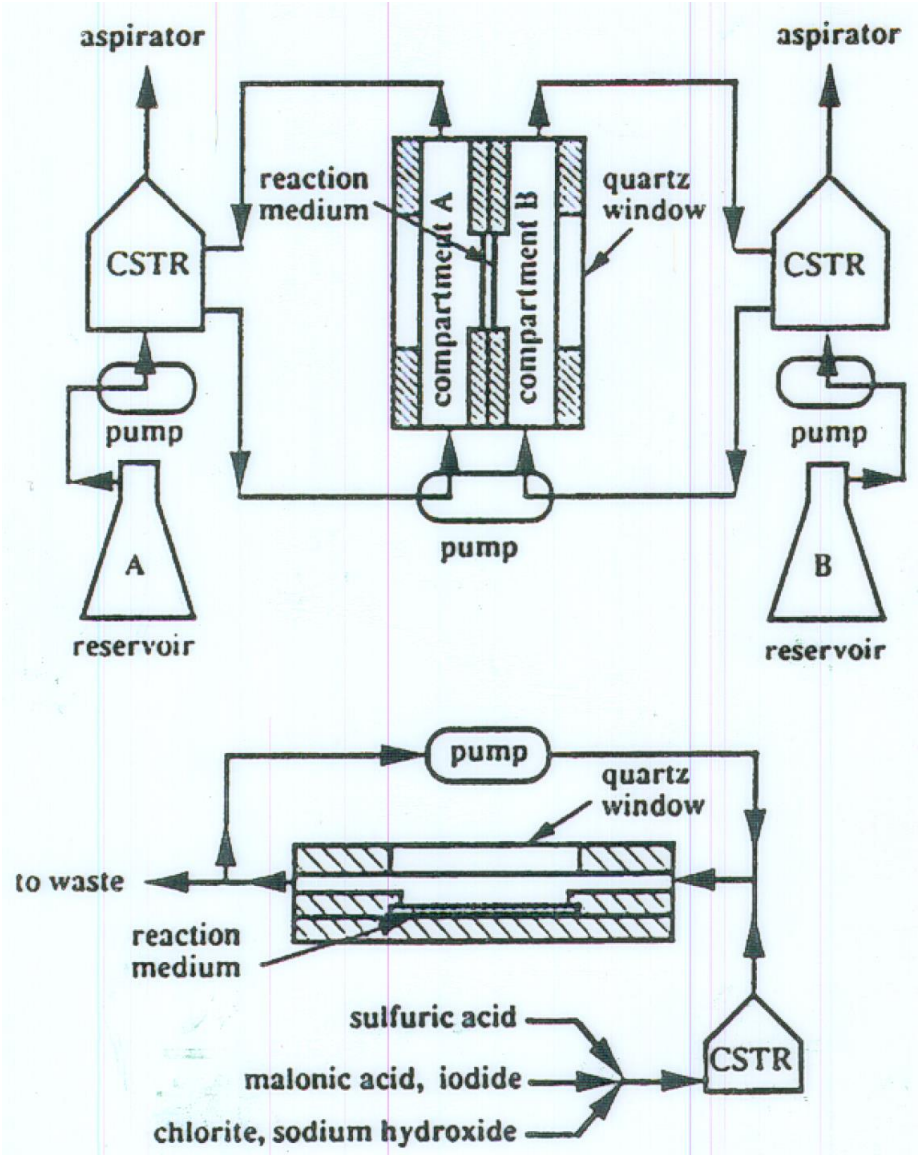
aspirator
aspirator
reaction medium
compartment A
compartment B
quartz window
CSTR
CSTR
pump
pump
pump
A
B
reservoir
reservoir
pump
quartz window
to waste
reaction medium
sulfuric acid
malonic acid, iodide
chlorite, sodium hydroxide
CSTR

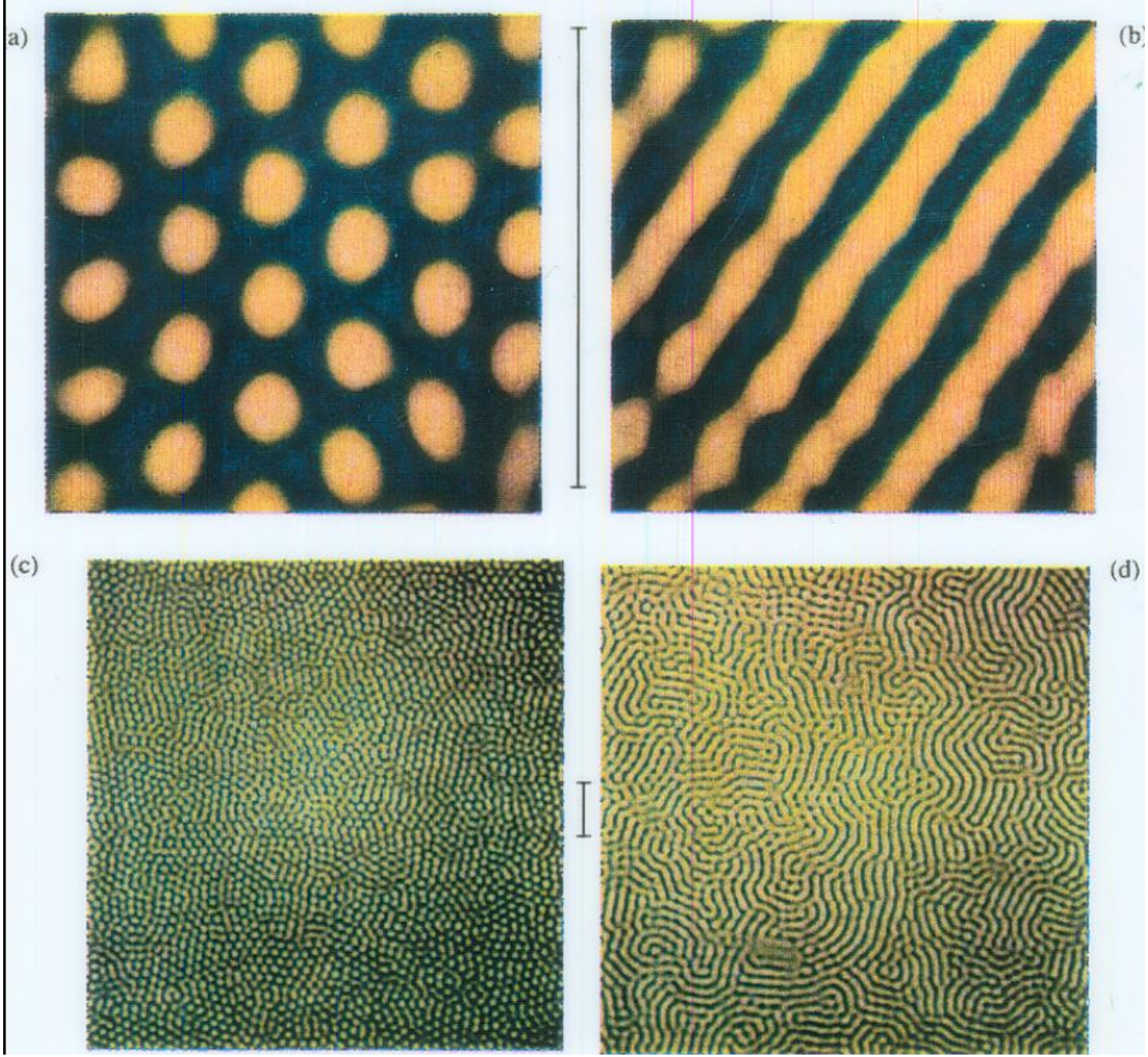
(a)
(b)
(c)
(d)

Properties/Predictions

- Minimum domain size for pattern
- Pattern complexity increases with domain size – limb experiments
- Effects of geometry – spots and stripes
- Developmental constraints

J.D. Murray

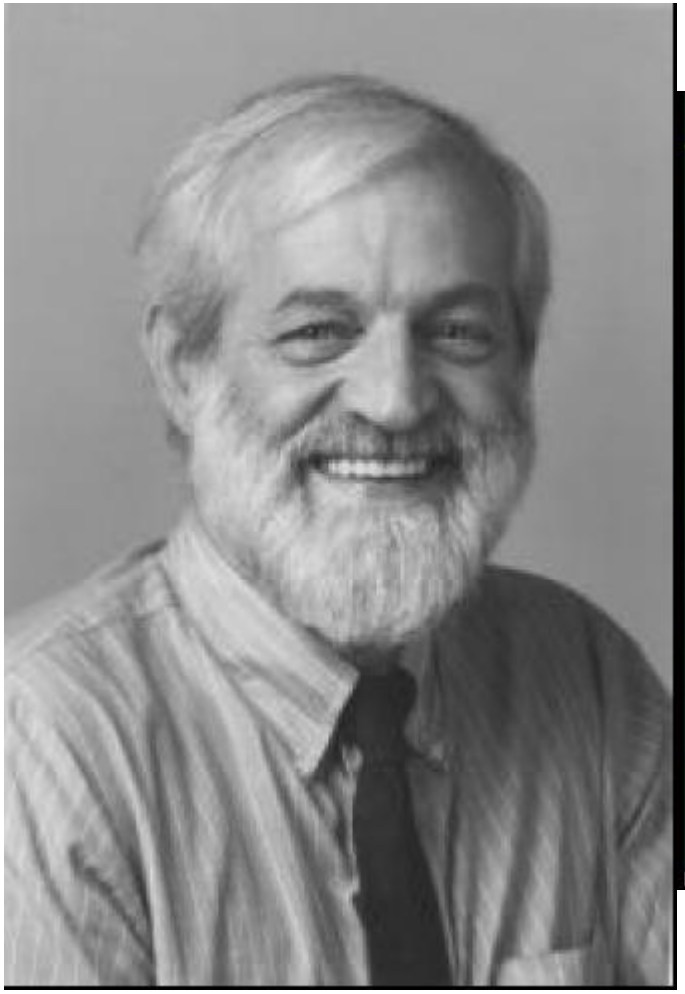

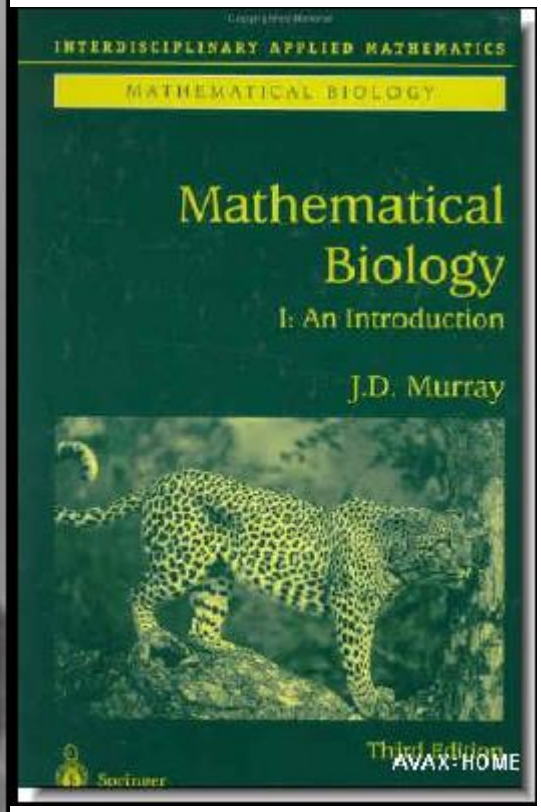
INTERDISCIPLINARY APPLIED MATHEMATICS
MATHEMATICAL BIOLOGY
Mathematical Biology
I: An Introduction
J.D. Murray
Third Edition
Springer
AVAX.HOME

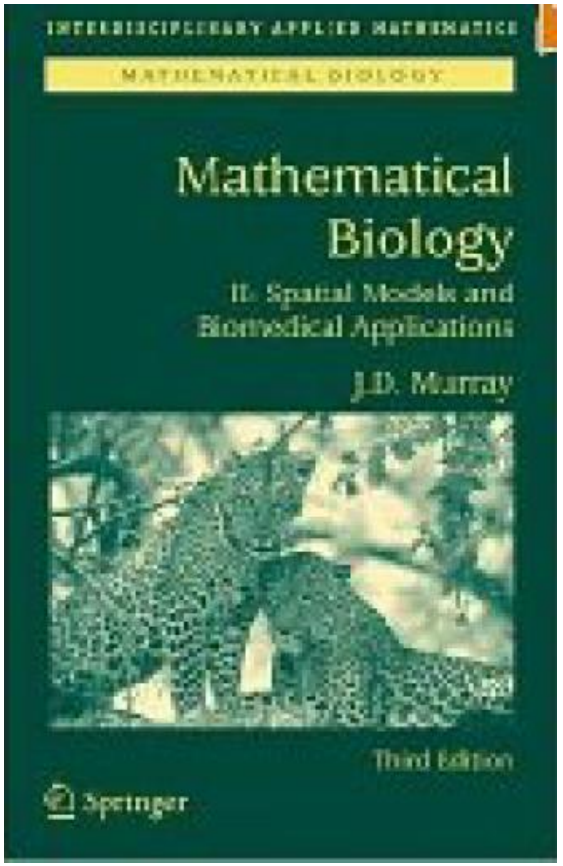
INTERDISCIPLINARY APPLIED MATHEMATICS
MATHEMATICAL BIOLOGY
Mathematical Biology
II: Spatial Models and Biomedical Applications
J.D. Murray
Third Edition
Springer

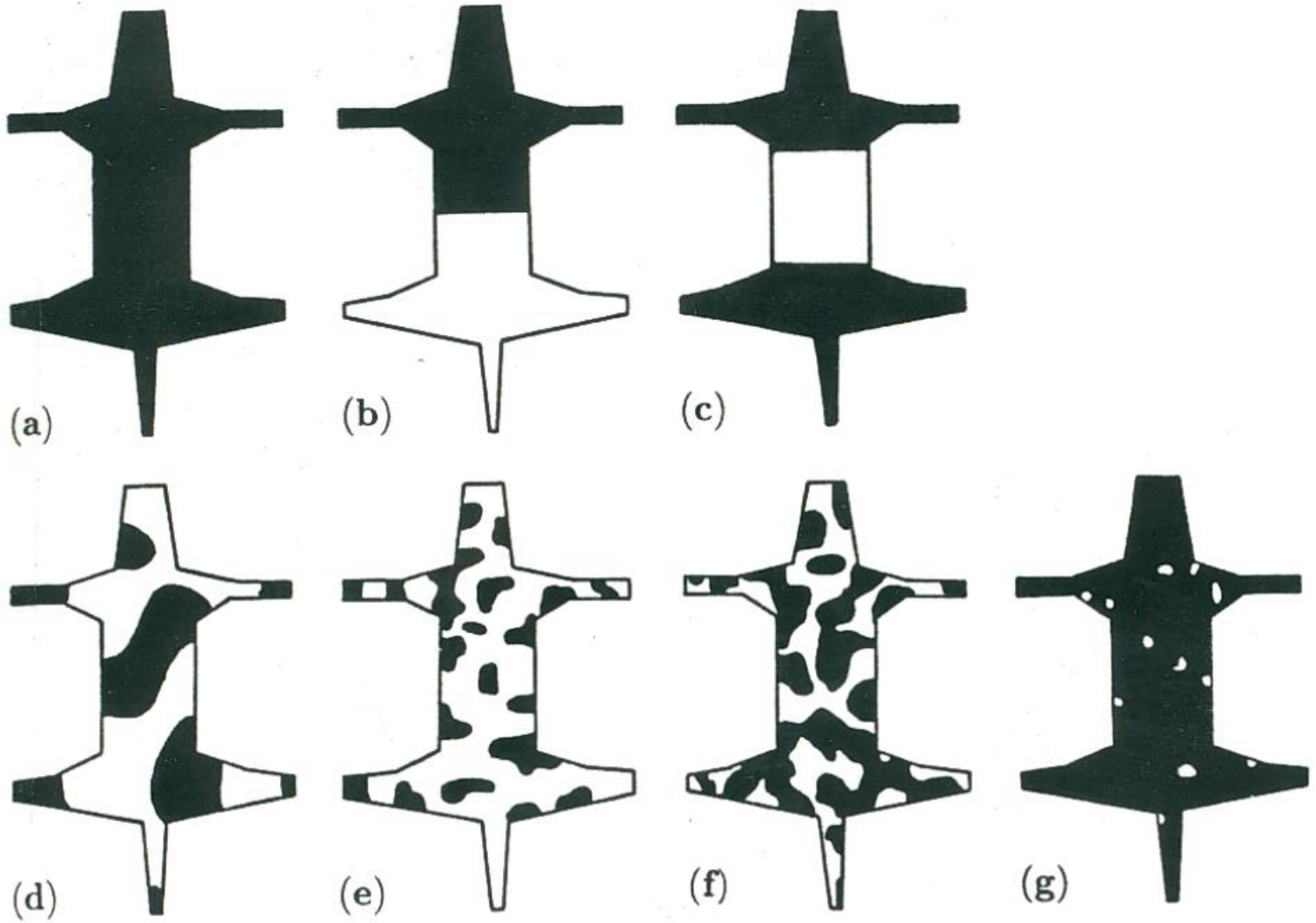
(a)
(b)
(c)
(d)
(e)
(f)
(g)

Belted Galloway

Tapering cylinder

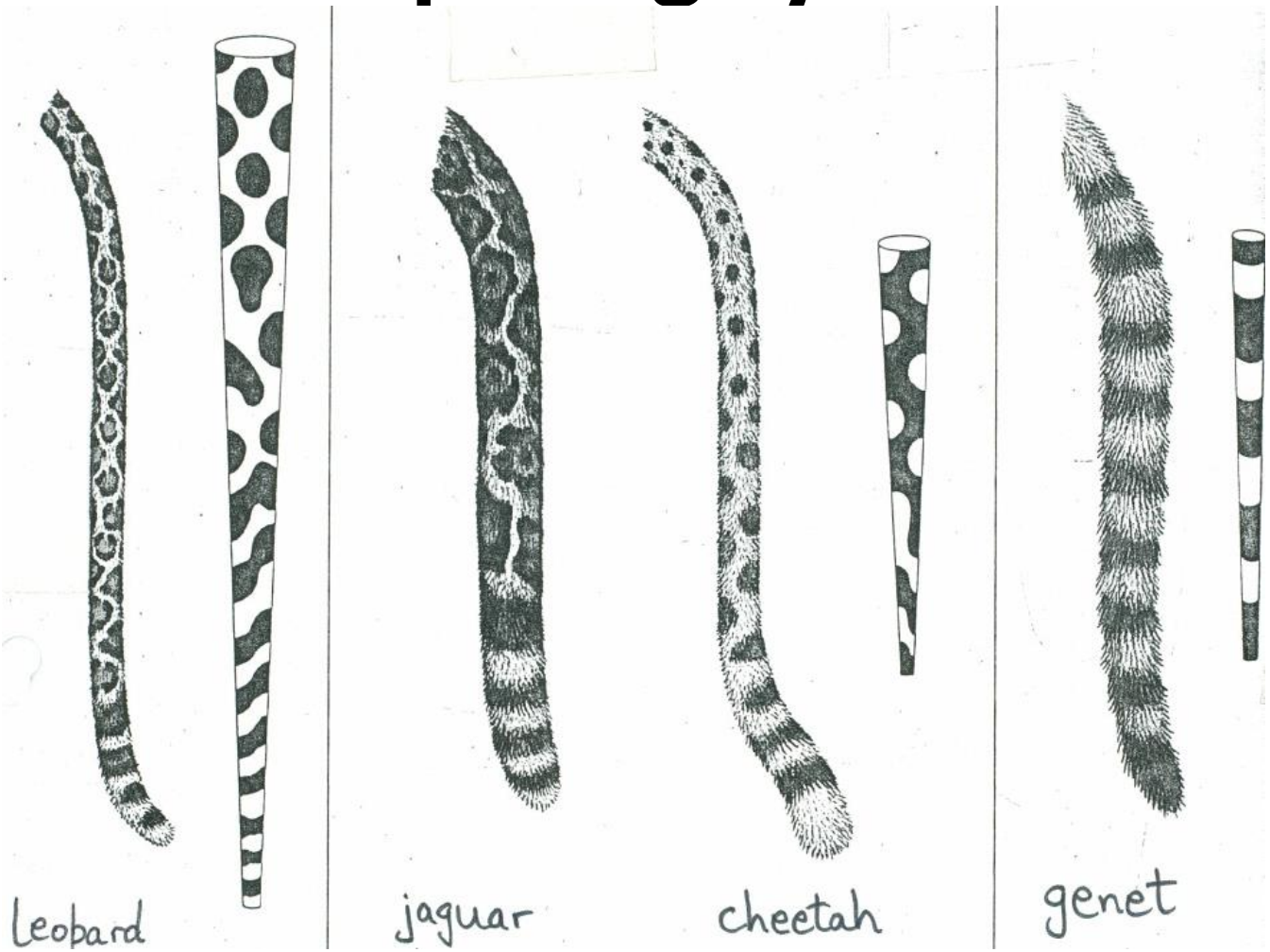

Developmental constraints

- The effect of domain geometry and size.

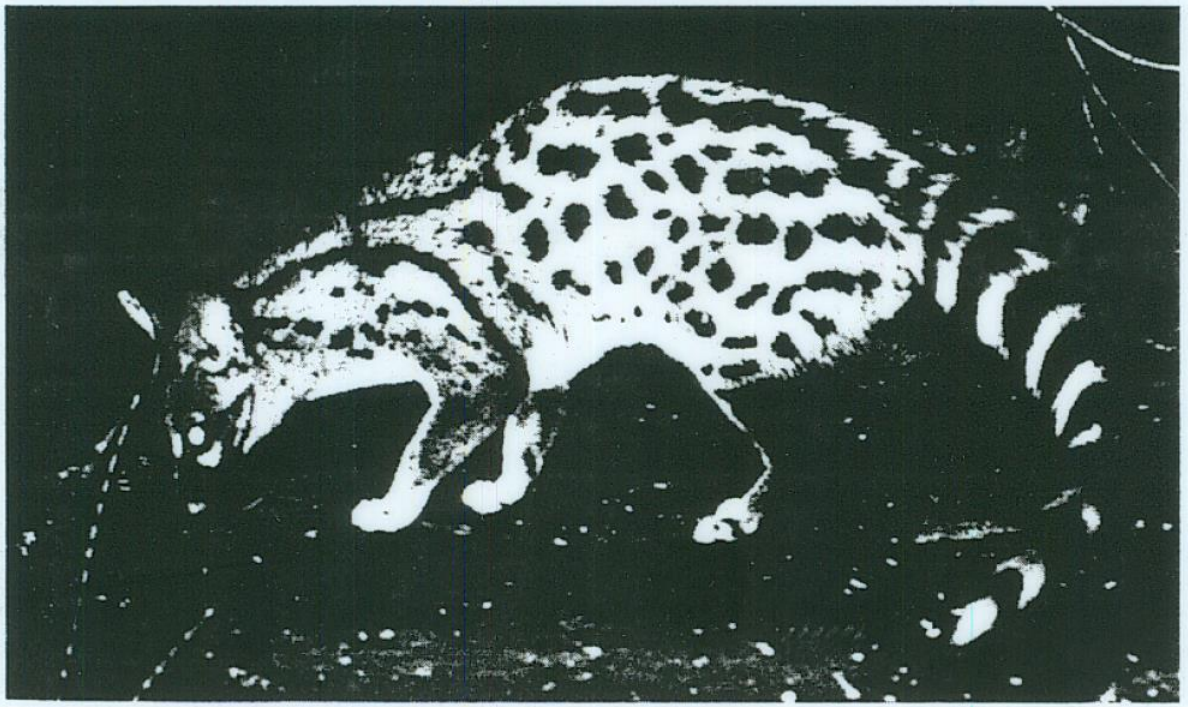

A common genet (*Genetta genetta*) showing the distinctly striped tail emerging from a spotted body. (Photograph courtesy of Hans Kruuk)

Developmental Constraint: Oster, Shubin, Murray, Alberch, Evolution and Morphogenesis Rules. The shape of the vertebrate limb in ontogeny & plylogency Evolution 45, 862-884, 1988


BECKHAM
32

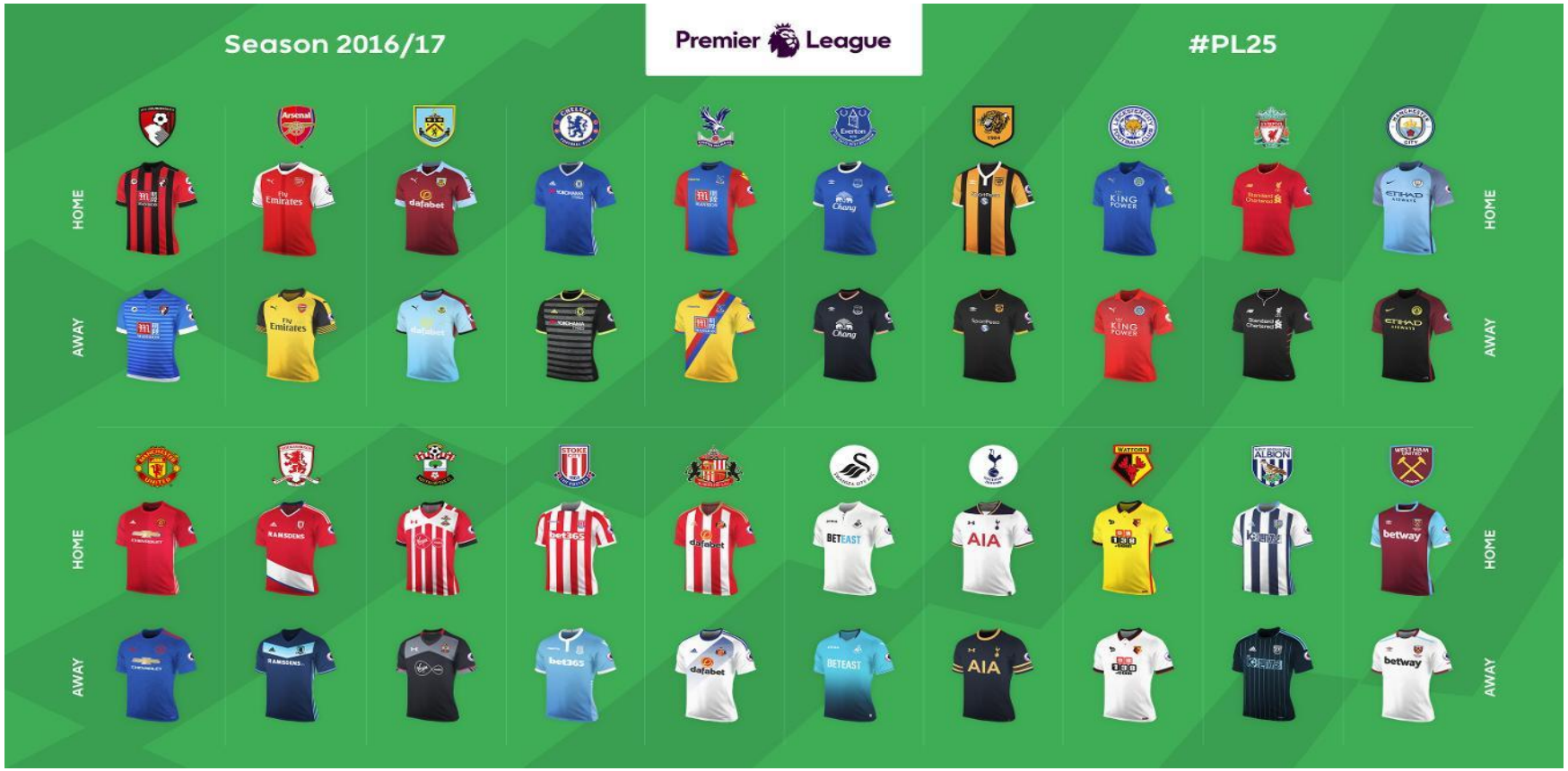
Season 2016/17
Premier League
#PL25
HOME
AWAY
HOME
AWAY
HOME
AWAY
HOME
AWAY

Experiments

- If we were to decrease/increase the domain size of the limb domain that produces digits would we obtain:
- Smaller/larger digits?
- Fewer/more digits?

The Turing model predicts the latter.

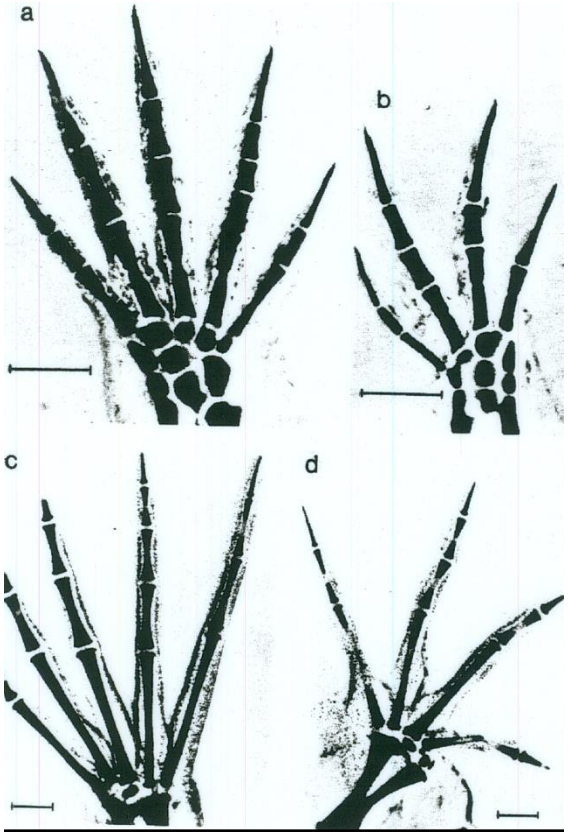

Fig. 18.7a-d. Experimentally induced alterations in the foot of the salamander Ambystoma mexicanum and the frog Xenopus laevis through treatment of the limb bud with colchicine. (a) Normal right foot of the salamander and (b) the treated left foot. (c) Normal right foot of the frog with (d) the treated left foot. (From Alberch and Gale 1983: photographs courtesy of P. Alberch)

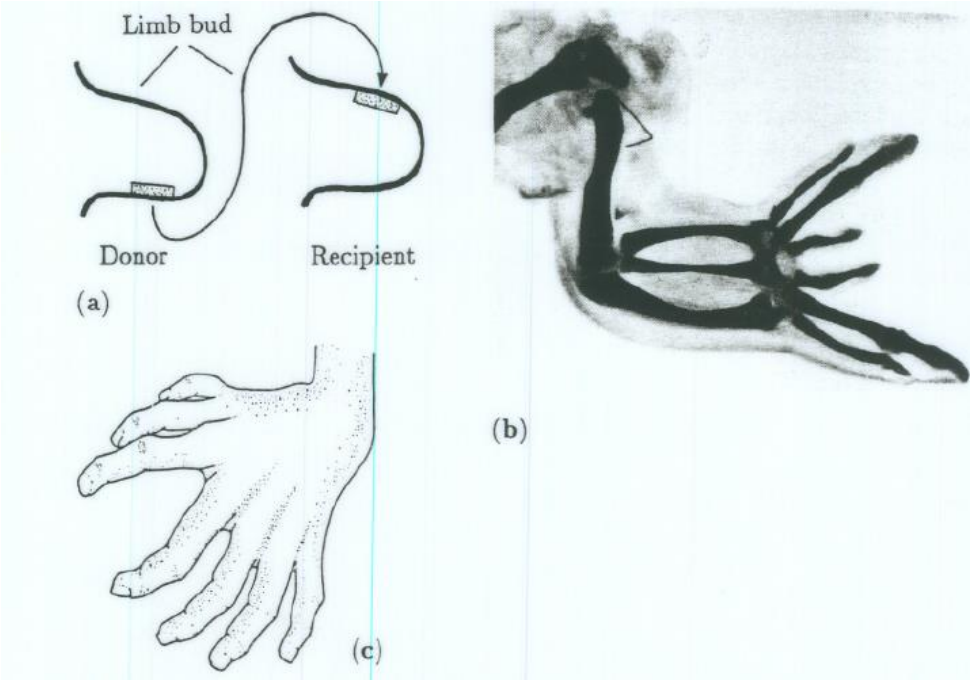

17.14a-c (a) Graft experiments involve taking a small piece of tissue from one limb bud and grafting it onto another. The effect of such a graft is to induce increased cell proliferation and hence increase the subsequent size of limb. The result is to induce growth commensurate with a domain in which multiple cell condensations can be fitted in at each stage of growth and hence result in double limbs. (b) Photograph of a double limb in a 10 day chick following an anterior graft of tissue from the posterior region, the zone of polarizing activity (ZPA), of another limb as in (a). The grafted tissue creates the appropriate symmetry which results in a mirror image limb. (From Wolpert and Hornburch 1987: photograph courtesy of L Wolpert and A. Hornburch) (c) A natural example of a double hand of a Boston man: note the lack of thumb and the mirror symmetry. (After Walbot and Holder 1987).

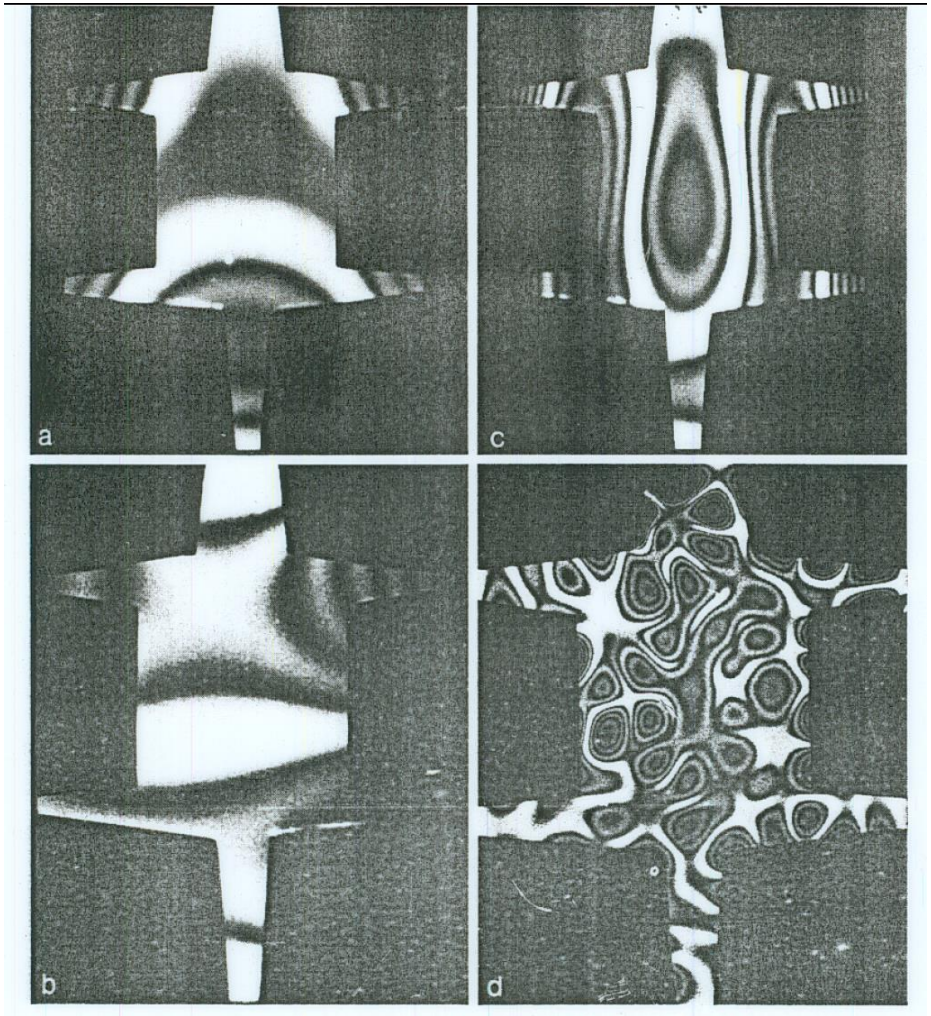

- J.D. Murray, Mathematical Biology, Springer 2002, 2003 (Xu, Vest, Murray, Appl. Optics, 22, 3479-3483 (1983) – vibrating plates.

Counter-examples

How do we explain this?

Hans Meinhardt, “The Algorithmic Beauty of SeaShells”

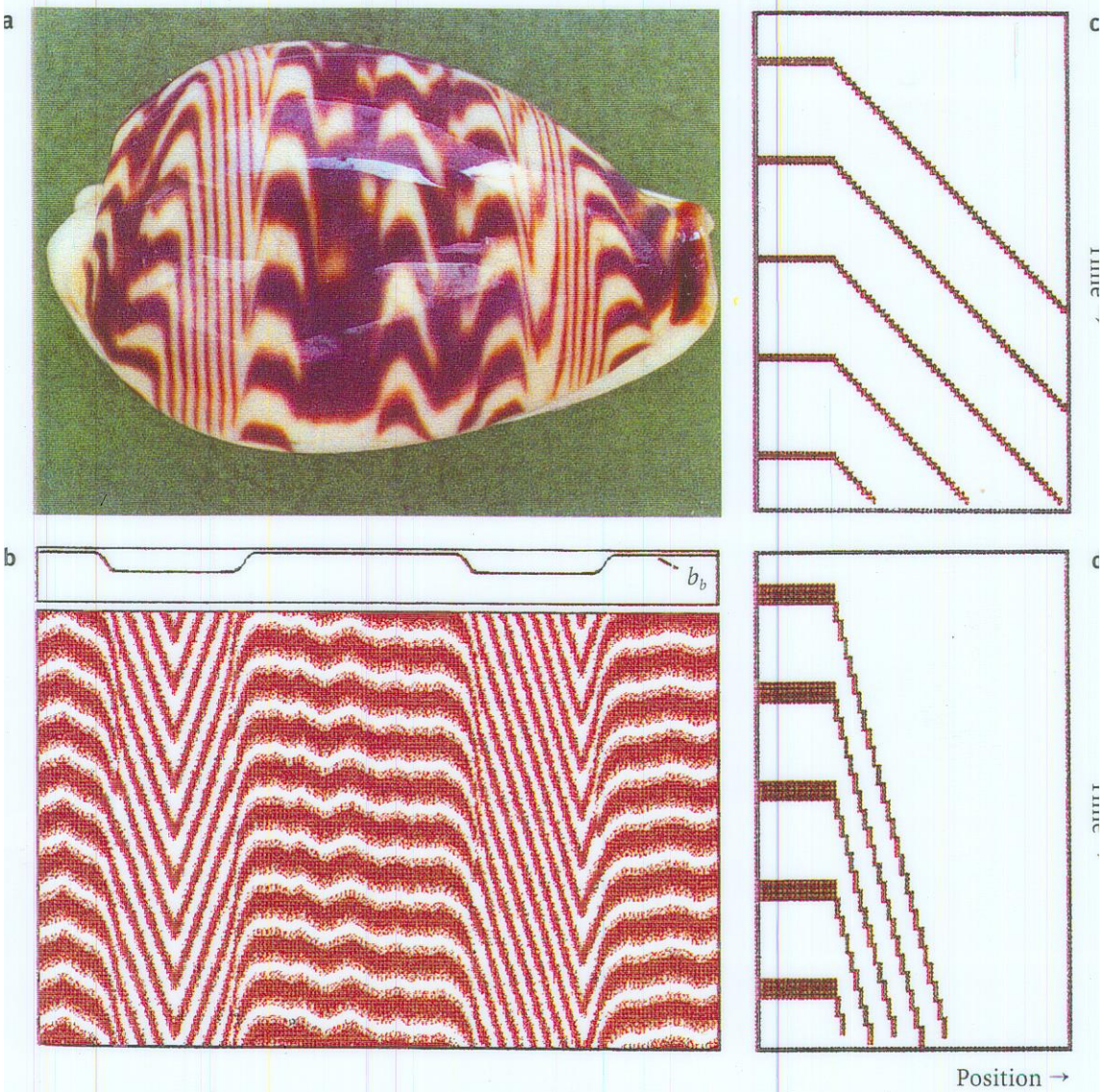

Figure 4.6. Steep lines. (a) Shell of *Cypraea diluculum*. (b) Model: if the activator autocatalysis has an upper bound (saturation), the activated period within a cycle is relatively long and the stripes are thick. If activator diffusion is low, the activation of one cell by its activated neighbour requires time. Since the activated portion of the cycle is long, more time is available in which one cell can infect its neighbour. Despite the large phase difference, this does not lead to wave termination. A large phase difference can accumulate between neighbouring cells. The result is thick lines in regions with high oscillation frequencies and very steep but narrow lines in regions with lower oscillation frequencies. (c,d) Schematic drawing to illustrate the connection between line width and maximum steepness; [S46].

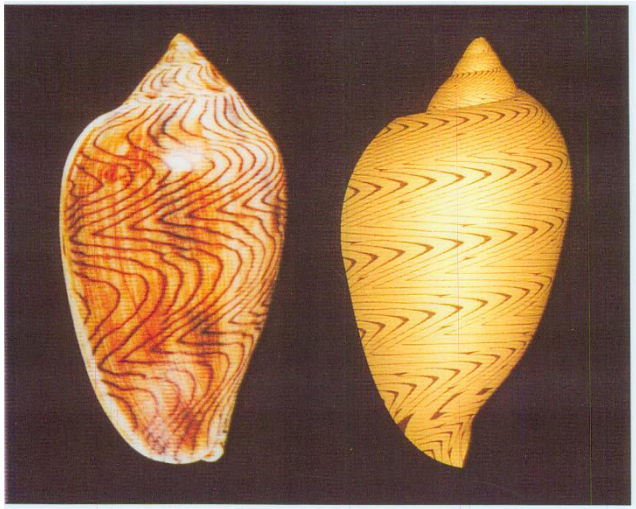

Figure 10.15. A photograph (see Sabelli, 1979) and model of *Amoria undulata* (Waved Volute)

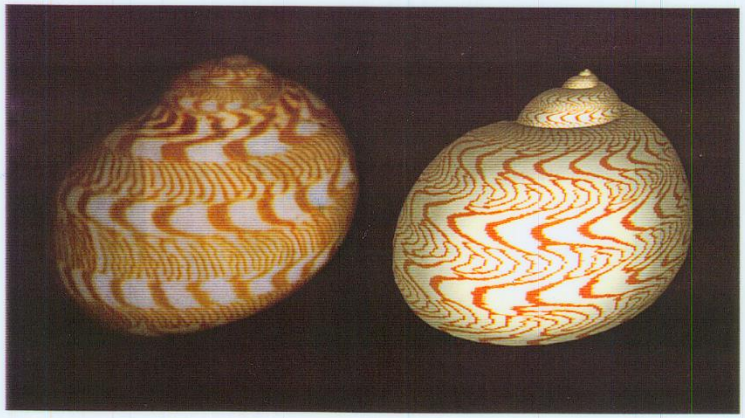

Figure 10.16. A photograph and model of *Natica euzona*

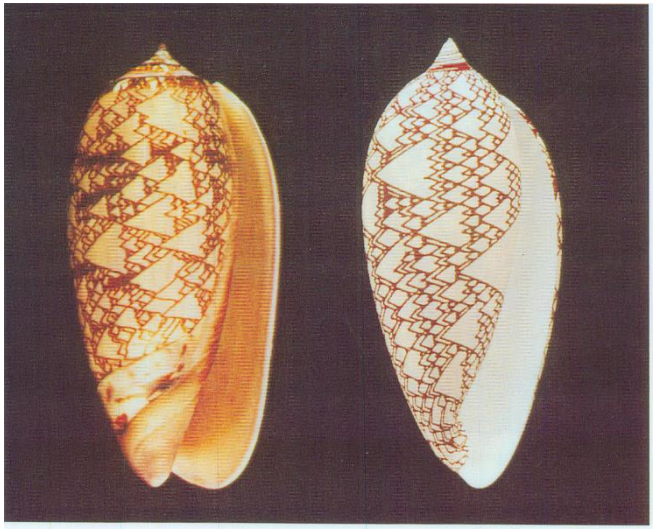

Figure 10.18. A photograph (see Sabelli, 1979) and model of *Oliva porphyria*

Conclusions

- Pattern can arise as an **emergent** property – that is, two stabilizing processes interact to give rise to an instability
- Turing proposed the idea of morphogens – these have been shown to exist
- Turing patterns arise in chemistry
- Do Turing patterns arise in biology?

Lewis Wolpert's French Flag Model (1969)

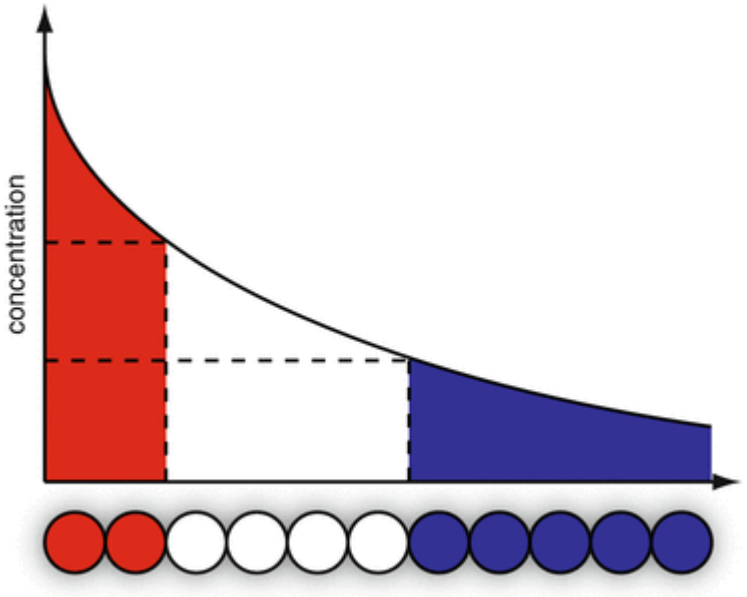

WOLPERT, L., & HORNBRUCH, A. 1990 Double anterior chick limb buds and models for cartilage rudiment specification. *Development* **109,** 961-6.

P - posterior

A – anterior

- So, they constructed a new limb bud which had the same size as the normal limb bud, but it gave two bones instead of one.

- The Turing model predicts that, as the domain size does not change, the pattern should not change

P.K. Maini, D.L. Benson, J.A. Sherratt, Pattern formation in reaction diffusion models with spatially inhomogeneous diffusion coefficients, IMA J.Math.Appl.Med. Biol. 9, 197-213 (1992)

$$u_t = \gamma f(u, v) + u_{xx}$$
$$v_t = \gamma g(u, v) + [D(x)v_x]_x,$$

$$c_t = v^2 c_{xx} - \theta^2 c$$

$c_x(0, t) = 0$, $c(1, t) = c_0$,

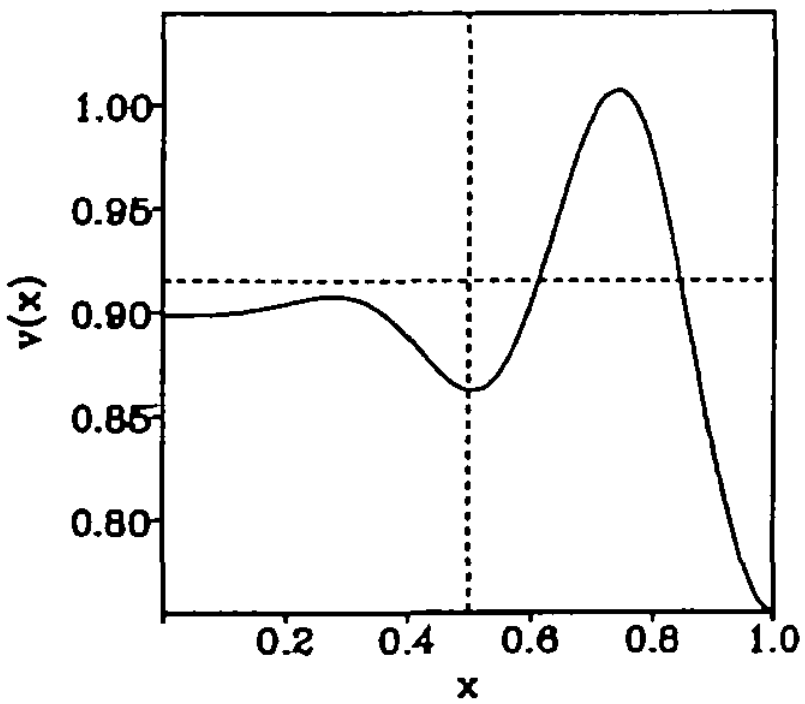
1.00
0.95
0.90
0.85
0.80
v(x)
0.2
0.4
0.6
0.8
1.0
x

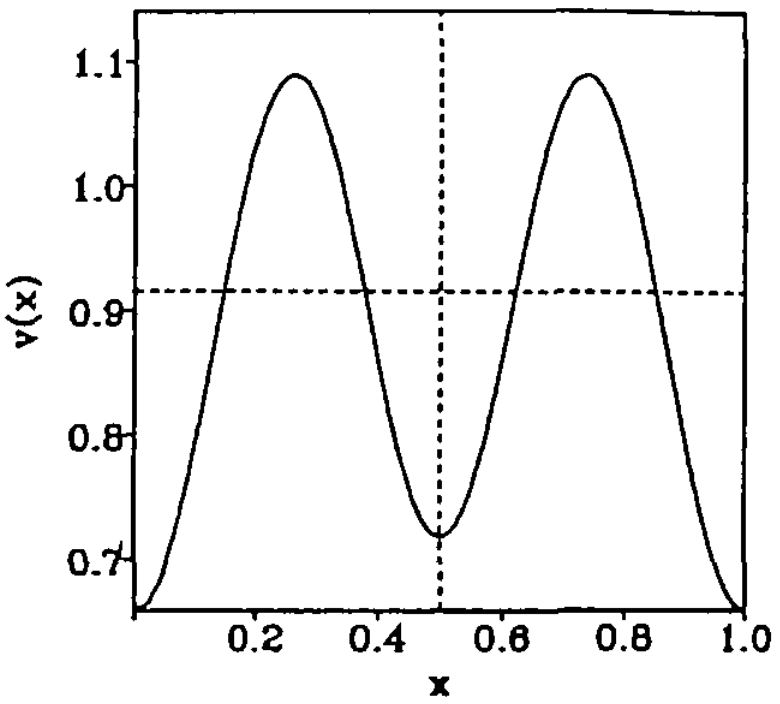
1.1
1.0
0.9
0.8
0.7
v(x)
0.2
0.4
0.6
0.8
1.0
x

- Therefore the model shows that the experiment would be consistent with the model if there was a gradient in diffusivity going from posterior to anterior

- BRUMMER, F., ZEMPEL, G., BUHLE, P., STEIN, J.-C, & HULSER, D. F. 1991 Retinoic acid modulates gap junctional permeability: A comparative study of dye spreading and ionic coupling in cultured cells. *Exp. Cell Res.* **196,** 158-63.

- Crucially, retinoic acid is produced at the zone of polarising activity (ZPA) in the limb bud and this is situated at the posterior end of the limb bud.

- So, D is high at anterior and low at posterior.

EFFECTS OF DOMAIN GROWTH (Kondo and Asai, Nature 1995)

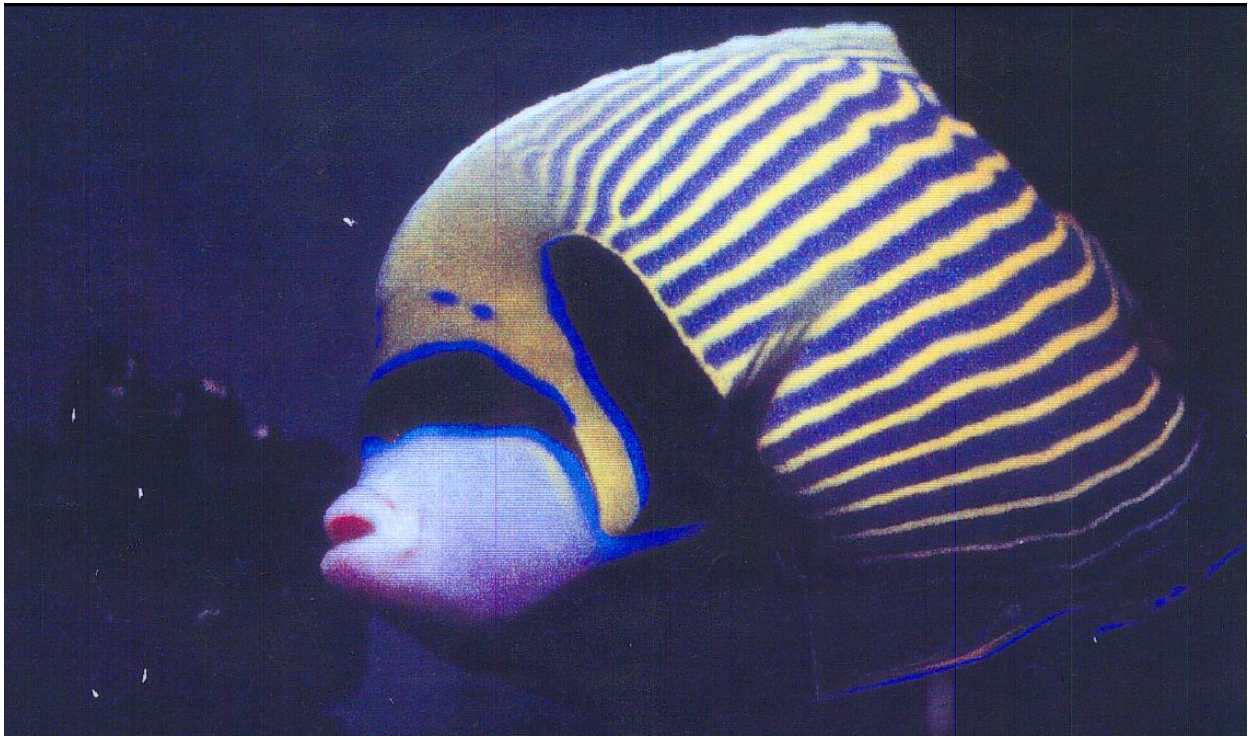

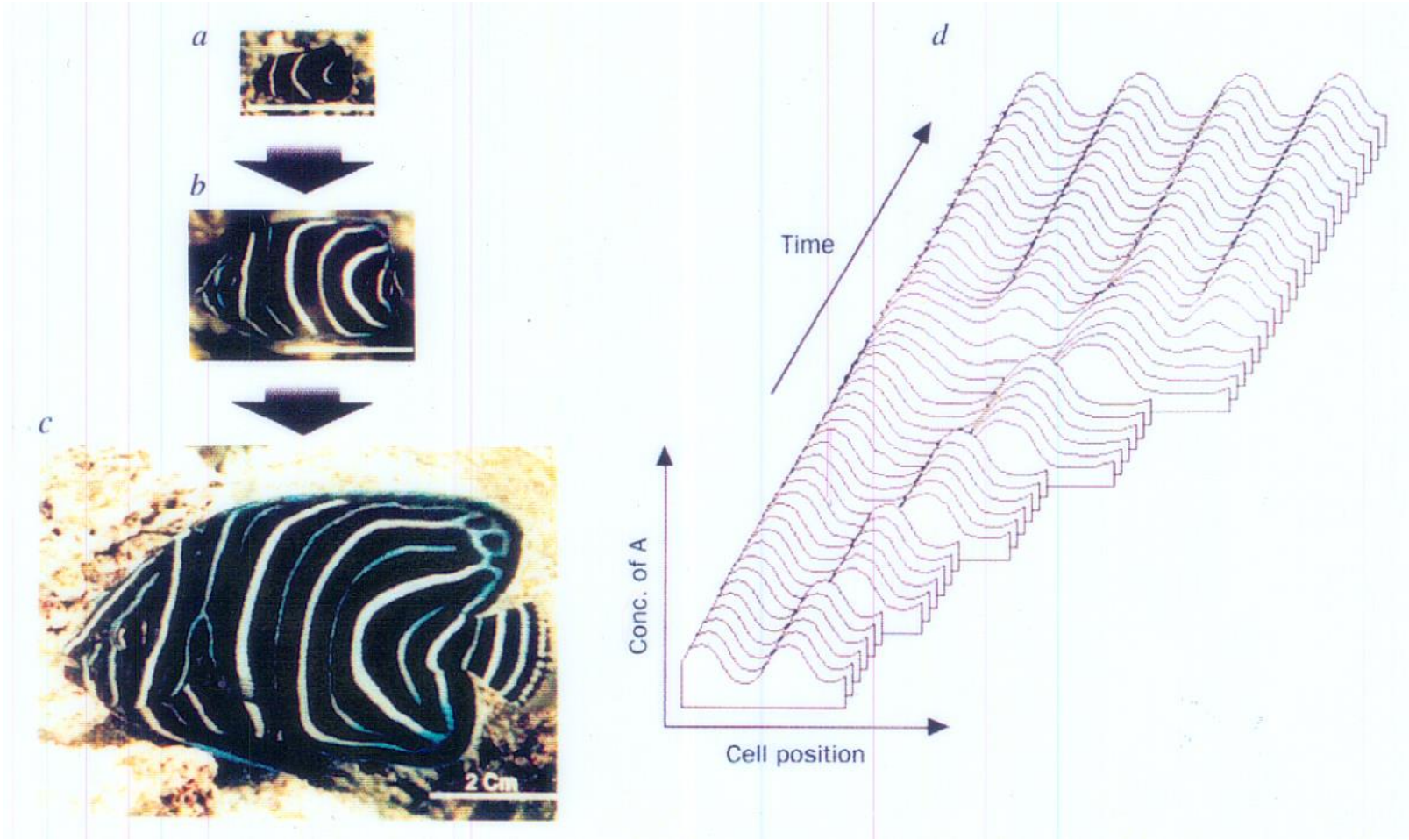

FIG. 1 Rearrangement of the stripe pattern of *Pomacanthus semicirculatus* and its computer simulation. *a–c*, Photographs of the juvenile of *P. semicirculatus*. Ages are ~2 months (*a*), ~6 months (*b*) and ~12 months (*c*). Scale bars, 2 cm. *d*, Computer simulation of the reaction–diffusion wave on the growing one-dimensional array of cells. One of the five cells is forced to duplicate periodically (once in 100 iterations). Concentration of activator is represented as the vertical height. The equations for calculation are as fo'lows:

$$\frac{dA}{dt} = c_1 A + c_2 I + c_3 - D_A \frac{d^2 A}{dx^2} - g_A A, \quad \frac{dI}{dt} = c_4 A + c_5 - D_I \frac{d^2 I}{dx^2} - g_I I$$

where A and I are the concentration of the activator molecule and the inhibitor molecule, respectively, D_A and D_I are the diffusion constants, g_A and g_I are the decay constants, and $D_A = 0.007$, $D_I = 0.1$, $g_A = 0.03$, $g_I = 0.06$, $c_1 = 0.08$, $c_2 = -0.08$, $c_3 = 0.05$, $c_4 = 0.1$, $c_5 = -0.15$. Upper and lower limits for the synthesis rates of the activator ($c_1 A + c_2 I + c_3$) and inhibitor ($c_4 A + c_5$) are set as $0 < c_1 A + c_2 I + c_3 < 0.18$ and $0 < c_4 A + c_5 < 0.5$. These upper and lower limits are set to avoid unrealistic situations. A moderate upper-limit value of the activator synthesis rate is required to get a pattern of stripes rather than spots[15] (spots are obtained if this value is exceeded). We used the kinetics of Turing[1]. Other stripe-forming interactions[12,15], in which the upper and lower limit is a natural outcome of the kinetics, can simulate the fish pattern rearrangement reported here.

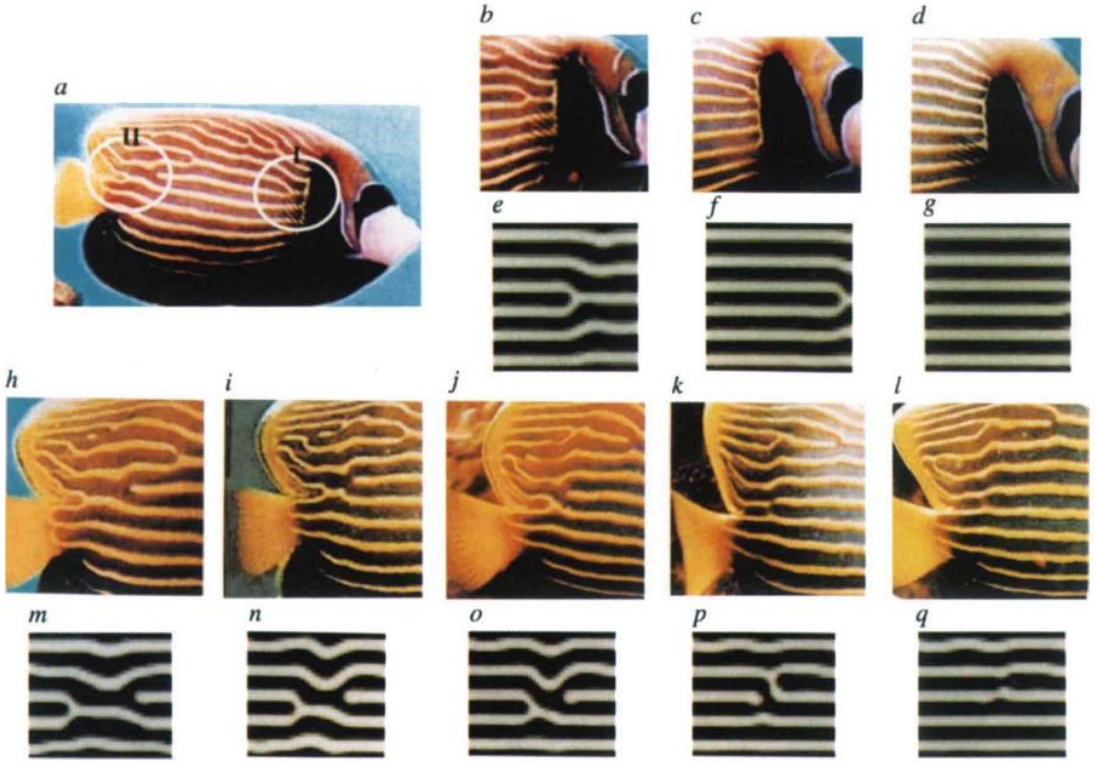

FIG. 2 Rearrangement of the stripe pattern of *Pomacanthus imperator* (horizontal movement of branching points) and its computer simulation. *a*, An adult *P. imperator* (~10 months old). *b*, Close-up of region I in *a*. *c*, *d*, Photographs of region I of the same fish taken two (*c*) and three (*d*) months later. *e*, Starting stripe conformation for the simulation (region I). *f*, *g*, Results of the calculation after 30,000 (*f*) and 50,000 (*g*) iterations. *h*, Close-up of region II in *a*. *i*–*l*, Photographs of region II of the same fish taken 30 (*i*), 50 (*j*), 75 (*k*) and 90 (*l*) days later, respectively. *m*, Starting stripe conformation for the simulation (region II). *n*–*q*, Results of the calculation after 20,000 (*n*), 30,000 (*o*), 40,000 (*p*) and 50,000 (*q*) iterations, respectively. Fish (Fish World Co. Ltd (Osaka)) were maintained in artificial sea water (Martin Art, Senju). Skin patterns were recorded with a Canon video camera and printed by a Polaroid Slide Printer. In the simulated patterns, darker colour represents higher concentrations of the activator molecule. Equations and the values of the constants used, as Fig. 1.

Robustness

- Turing patterns are not robust – small changes in initial conditions can lead to changes in pattern. Bard and Lauder, How well does Turing's theory of morphogenesis work? J. Theor. Biol., 45, 501-531, 1974

Bulletin of Mathematical Biology (1999) **61**, 1093–1120
Article No. bulm.1999.0131
Available online at http://www.idealibrary.com on IDEAL

Reaction and Diffusion on Growing Domains: Scenarios for Robust Pattern Formation

EDMUND J. CRAMPIN*, EAMONN A. GAFFNEY AND PHILIP K. MAINI

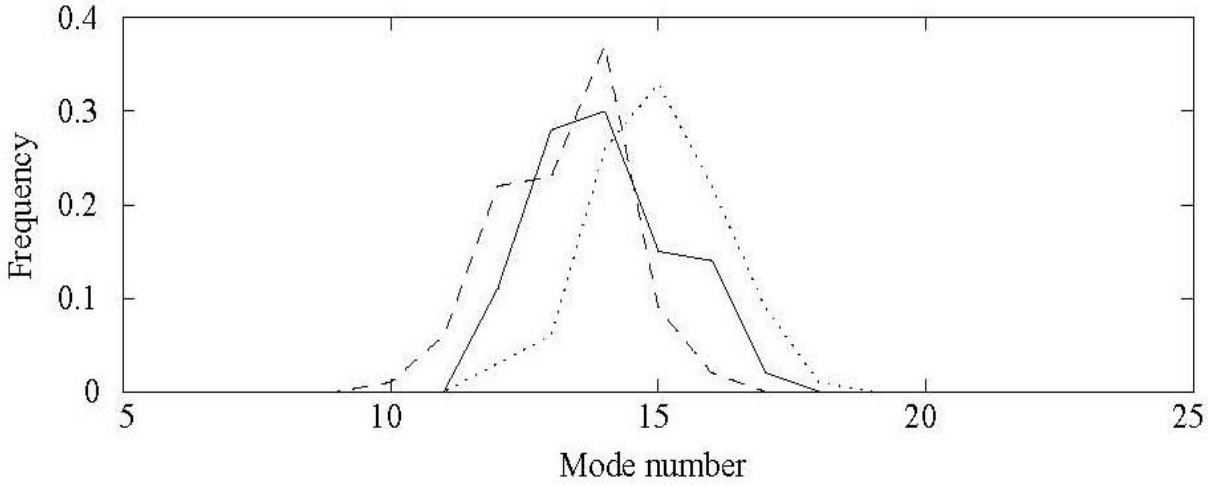

Figure 1. Relative frequencies of steady state solution modes against mode number m for numerical simulation of a reaction–diffusion equation (1) with Schnakenberg kinetics (24) for three different values of γ. Each simulation took different random initial conditions with zero flux boundary conditions. Dashed, solid and dotted lines correspond to $\gamma = 190$, 215 and 240 for which the fastest growing linear mode is $m = 15$, 16 and 17, respectively.

3. Reaction and Diffusion on Growing Domains

In this section we derive the evolution equations describing the interaction of n chemical species reacting in and diffusing through a growing domain Ω_t. The conservation equation in integral form is given by

$$\frac{\mathrm{d}}{\mathrm{d}t}\int_{\Omega_t} c(\mathbf{x},t)\mathrm{d}\mathbf{x} = \int_{\Omega_t} \left[-\nabla\cdot\mathbf{j} + R(c)\right]\mathrm{d}\mathbf{x}, \tag{9}$$

where $\mathbf{j}$ is the flux. We use the Reynolds transport theorem to evaluate the left-hand side:

$$\frac{\mathrm{d}}{\mathrm{d}t}\int_{\Omega_t} c(\mathbf{x},t)\mathrm{d}\mathbf{x} = \int_{\Omega_t}\left[\frac{\partial c}{\partial t} + \nabla\cdot\mathbf{u}c\right]\mathrm{d}\mathbf{x} \tag{10}$$

where $\mathbf{u}(\mathbf{x},t)$ is the flow and, nondimensionalizing, we recover the evolution equation

$$\frac{\partial c}{\partial t} + \nabla\cdot(\mathbf{u}c) = \frac{D_1}{\omega L^2}\mathcal{D}\nabla^2 c + R(c). \tag{11}$$

Geirer-Meinhardt and Schakenberg

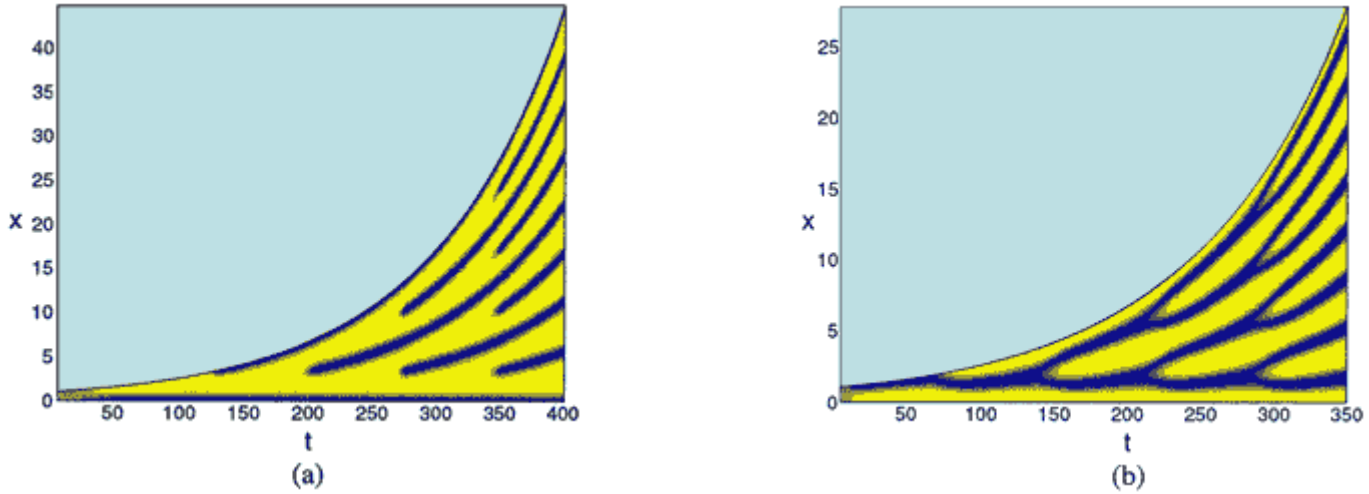

Patterns in the activator obtained on the uniformly growing domain. For domain expansion the patterns change regularly through mode doubling behaviour: (a) Gierer-Meinhardt kinetics, where showing regular insertion of new activator peaks and (b) Schnakenberg kinetics, where showing peak splitting.

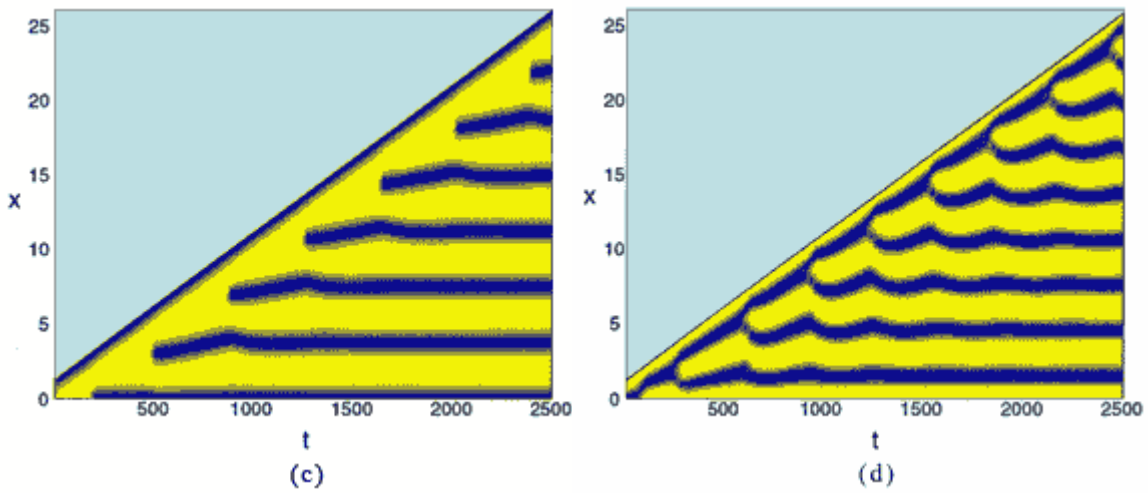

Figure 2. Patterns in the activator concentration obtained under apical growth for (c) Gierer-Meinhardt kinetics showing insertion of new activator peaks near the moving boundary and (d) Schnakenberg kinetics showing splitting of the activator peak proximal to the boundary.

Robustness

- Growth can enhance robustness of certain patterning modes at the expense of others.

- A.L. Krause et al, Recent progresss and open frontiers in Turing’s theory of morphogenesis,

Phil. Trans. R. Soc A 379(2213) 2021

Travelling Waves

Neural Crest

- A transient embryonic structure in vertebrates that gives rise to most of the peripheral nervous system and several non-neural cell types (muscle cells in the cardiovascular system, pigment cells, etc etc)
- Cranial, Trunk, Vagal and sacral (enteric nervous system), Cardiac

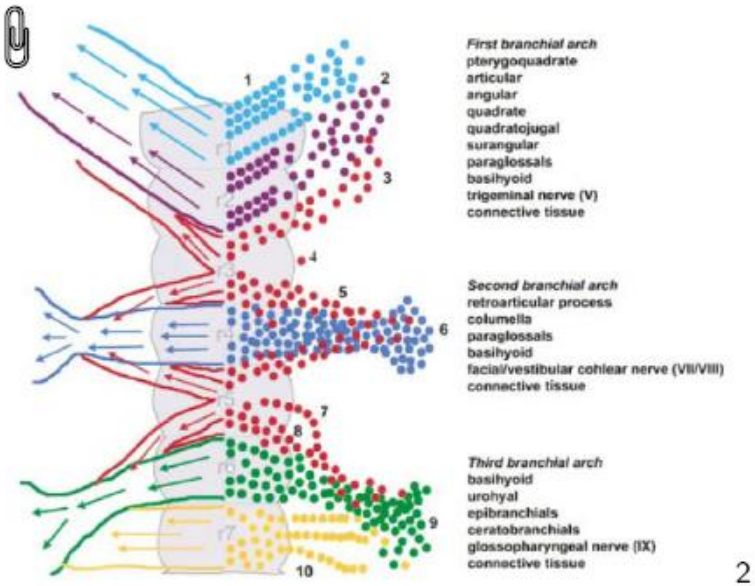

2

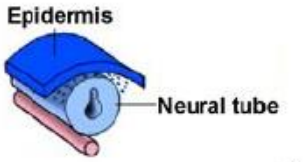

1

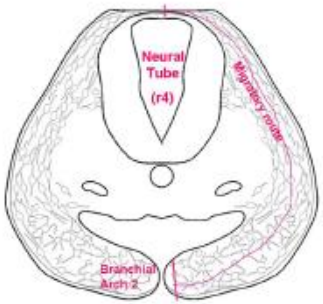

3

---

[1] Spicher and Michel (2007)

[2] Kulesa *et al.* (2004)

[3] Courtesy of P. M. Kulesa, Stowers Institute

Why Study This?

- 66 neural crest related diseases
- Nearly one-third of all birth defects occur as a result of improper patterning of the neural crest and associated vasculature
- Very similar in behaviour to the highly aggressive cancers, melanoma and neuroblastoma – serves as a powerful paradigm and is experimentally tractable
- R. Giniunaite, R.E. Baker, P.M. Kulesa, P.K. Maini, Modelling collective cell migration: neural crest as a model paradigm, J Math. Biol., 80, 481-504 (2020)

Stowers Institute for Medical Research

Paul Kulesa and Rebecca McLennan

With Ruth Baker and David Kay (Oxford)

Louise Dyson (now at Warwick)

Linus Schumacher (now at Edinburgh)

Rasa Giniunaite (Vilnius)

Duncan Martinson, Helen Byrne (Oxford)

Neural Crest

- A transient embryonic structure in vertebrates that gives rise to most of the peripheral nervous system and several non-neural cell types (muscle cells in the cardiovascular system, pigment cells, etc etc)
- Cranial, Trunk, Vagal and sacral (enteric nervous system), Cardiac

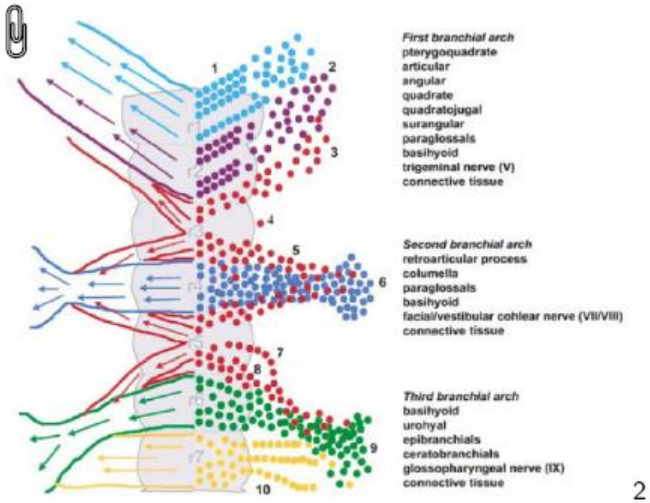

2

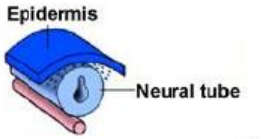

1

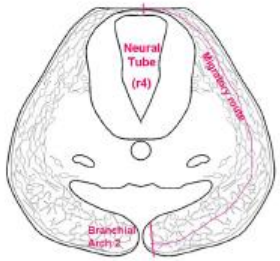

3

[1] Spicher and Michel (2007)

[2] Kulesa *et al.* (2004)

[3] Courtesy of P. M. Kulesa, Stowers Institute

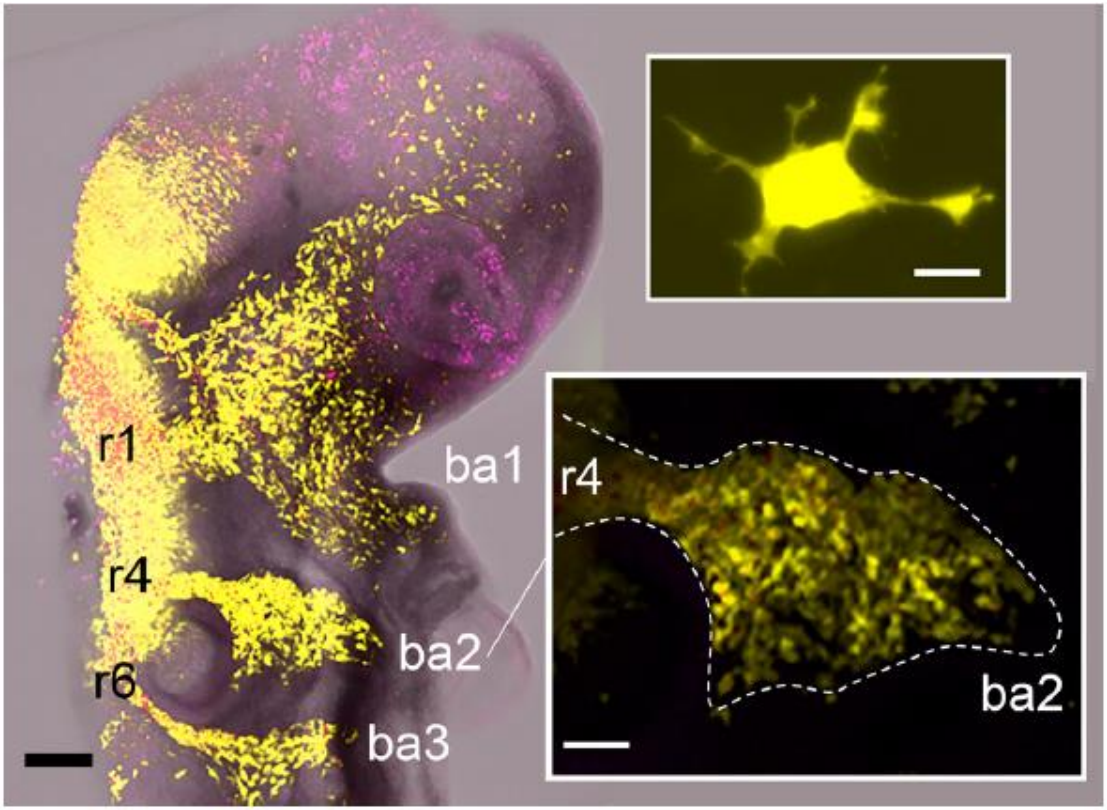
r1
r4
r6
ba1
ba2
ba3
r4
ba2

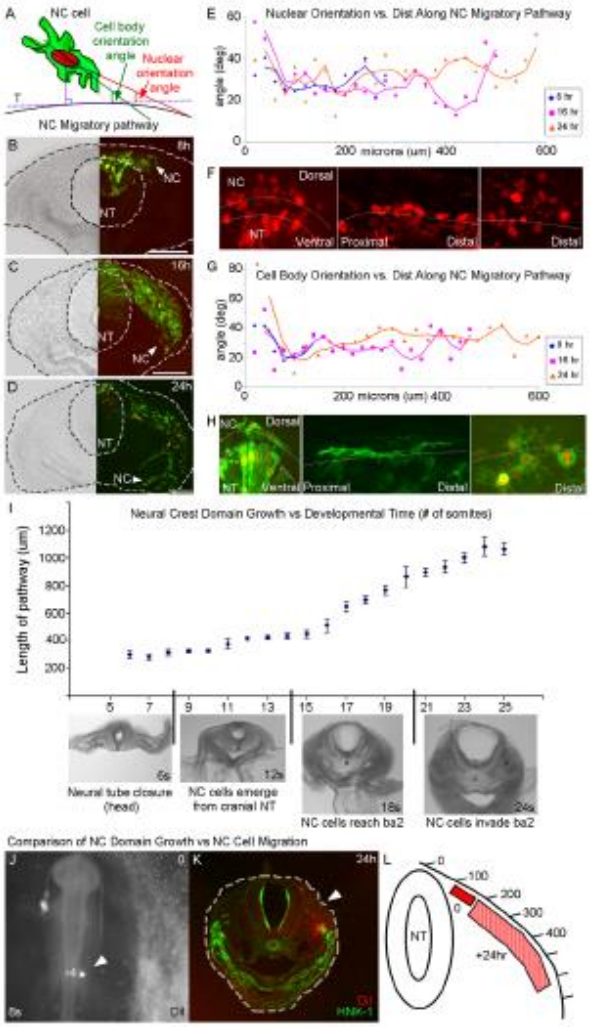

Fig. 1. NC cell direction is acquired after cells exit the neural tube and cells move faster than non-linear tissue growth. (A) Orientation angle measurements. (B-D) Typical projected images from 3D confocal z-stacks of transverse sections through the r4 NC cell migratory stream at 8, 16 and 24 hours after electroporation. (E) Average nuclear orientation angle with respect to distance along the migratory route from 8- (n=318 cells, 29 embryos), 16- (n=346 cells, 15 embryos) and 24- (n=240 cells, 25 embryos) hour data. (F) Representative images of migratory NC cells. (G) Average cell body orientation angle with respect to distance along the migratory route for 8- (n=89 cells, 10 embryos), 16- (n=254 cells, 27 embryos) and 24- (n=248 cells, 11 embryos) hour data. (H) Gap43-EGFP membrane-labeled NC cells. (I) Average length of the NC cell migratory domain at increasing developmental times. (J) Focal injection (arrowhead) of DiI into the lateral mesoderm prior to NC cell emigration. (K) Twenty four hours after injection in J. Arrowhead indicates site of injection. (L) Average spread of DiI-labeled tissue. Scale bars: 100 μm. NC, neural crest; NT, neural tube.

Model Hypothesis

- Can a chemoattractant (VEGF – vascular endothelial growth factor) produced by the overlying ectoderm be sufficient for robust invasion?
- Reaction-diffusion partial differential equation for VEGF with saturating (logistic) source production and sink terms for the cells.
- Assume a sink at the boundary (Homogeneous fixed (Dirichlet) BCs -- later on we use zero flux conditions) [Versican in Xenopus – Szabo et al, 2016, J. Cell. Biol.]
- Cells are discrete entities – sense the gradient and move with constant speed in direction of increasing VEGF

Model Equations

- solve chemoattractant RDE

$$\frac{\partial c}{\partial t} = D\left(\frac{1}{L^2}\frac{\partial^2 c}{\partial x^2} + \frac{\partial^2 c}{\partial y^2}\right) - c\sum_{i=1}^{N(t)} \frac{\lambda}{2\pi R^2} \exp\left[-\frac{L^2(x-x_i)^2 + (y-y_i)^2}{2R^2}\right] + \chi c(1-c) - \frac{\dot{L}}{L}c$$

diffusion | internalisation | production | dilution

- grow tissue

$$L_x(t) = L_0\left(\frac{L_\infty e^{a(t-t_s)L_\infty}}{L_\infty - 1 + e^{a(t-t_s)L_\infty}} + 1 - \frac{L_\infty e^{a(-t_s)L_\infty}}{L_\infty - 1 + e^{a(-t_s)L_\infty}}\right)$$

Hypothesis Test

- Can a chemoattractant (VEGF) produced by the overlying ectoderm be sufficient for robust invasion? **NO**

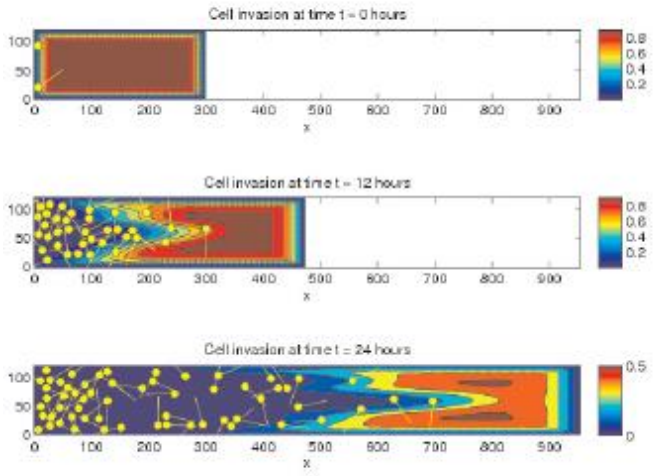

Keller-Segel Model

$$\frac{\partial n}{\partial t} = D_n \frac{\partial^2 n}{\partial x^2} - \frac{\partial}{\partial x}\left(n\,\chi(c)\frac{\partial c}{\partial x}\right)$$

$$\frac{\partial c}{\partial t} = D_c \frac{\partial^2 c}{\partial x^2} + f(n,c)$$

$$\chi(c) = \frac{K}{c}$$

Hypothesis Generation: “Leaders and Followers”

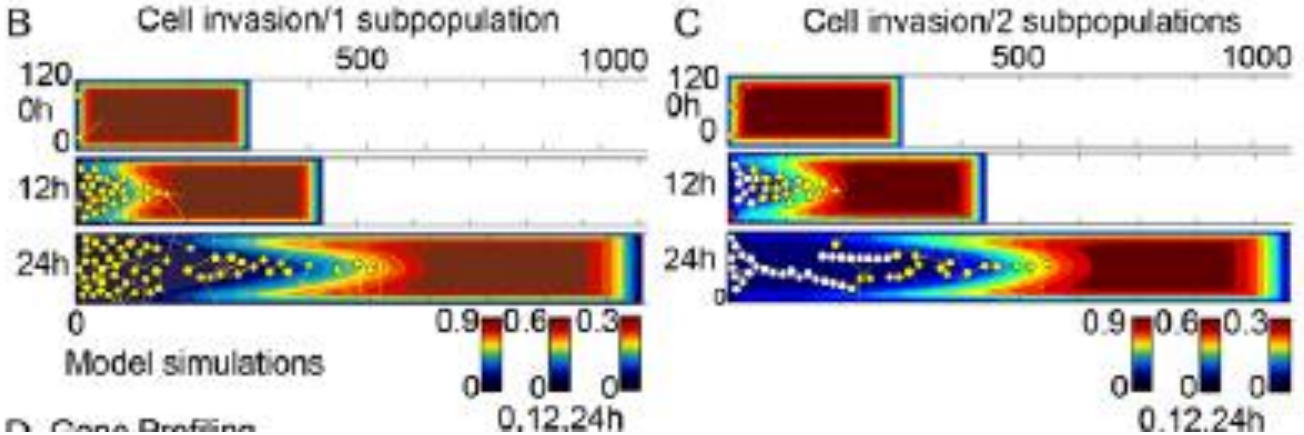

Model Prediction and Validation

- A single chemotactic gradient with a single cell type is not a feasible mechanism. There must be at least 2 cell types – one chemotactic, one not chemotactic.

- By FACS (flow cytometry analysis) and by LCM (laser capture microdissection) show significant differences in expression of a large number of genes.

- Leading NC cells have upregulated expression of cell guidance and navigation genes (cell guidance factor receptors [EphA4]; integrins (Itgb5); MMPs [MMP2]). Trailing cells have upregulated expression of cadherins distinct from leading NC cells in particular cadherin 11 upregulated at the front, cadherin 7 upregulated at the back.

- Cadherins code for adhesiveness (stickiness) so these experimental results show that the cells at the back are more sticky then the cells at the front, in agreement with the model.

Bioinformatics meets mathematical modelling

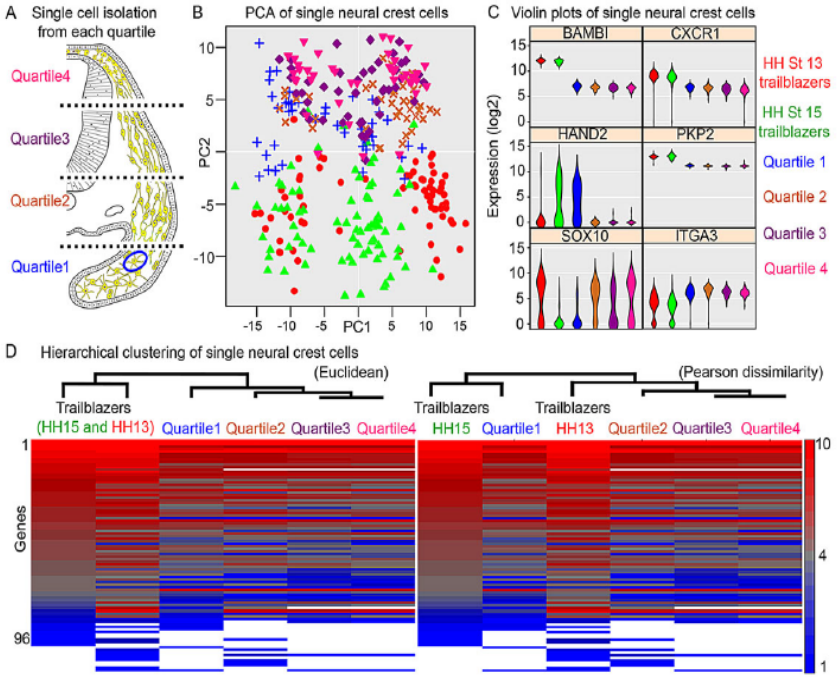

Fig. 6. Single trailblazer NC cells have a unique molecular profile. (A) Isolation of single NC cells (blue circle) from each quartile of the cranial NC stream. (B) PCA of single trailblazer and quartile NC cells. (C) Violin plots of selected genes. (D) Hierarchical clusterings of single trailblazer and quartile NC cells by Euclidean distance or Pearson dissimilarity based upon averages of the 96-gene profiles. *n*=318 cells total: *n*=72 HH stage 13 trailblazers, *n*=76 HH stage 15 trailblazers, *n*=43 quartile 1, *n*=41 quartile 2, *n*=44 quartile 3 and *n*=42 quartile 4.

Further Complications

- Growth is NOT spatially uniform**!** McKinney et al, Dev. Biol., 461, 184-196 (2020)
- Growth is partly induced by the NC cells.
- Gradient of phenotypes (ongoing)
- Boundary Conditions
- Leaders can break away

References

- R. McLennan et al, Multiscale mechanisms of cell migration during development: theory and experiment, Development. 139, 2935-2944 (2012)
- R. McLennan et al, Neural crest migration is driven by a few trailblazer cells with a unique molecular signature narrowly confined to the invasive front, Development, 142, 2014-2025, (2015)
- L.J. Schumacher et al, Multidisciplinary approaches to understanding collective cell migration in developmental biology, Open Biol., 6, 160056 (10) pages, (2016)
- McLennan et al, DAN (NBL1) promotes collective neural crest migration by restraining uncontrolled invasion, J. Cell Biology, 216(10), 3339-3354 (2017)

- R. Giniunaite et al, Modelling collective cell migration: neural crest as a model paradigm, J Math. Biol., 80, 481-504 (2020)
- M.C. McKinney et al, Visualizing mesoderm and neural crest cell dynamics during chick head morphogenesis, Dev. Biol., 461, 184-196 (2020)
- R. McLennan et al, Colec12 and Trail signaling confine cranial neural crest cell trajectories and promote collective cell migration, Dev. Dynamics, 252:629–646 (2023)

R. McLennan et al, Neural crest cells bulldoze through the microenvironment using Aquaporin 1 to stabilize filopodia, (2020) Development, 147

THANK YOU FOR YOUR ATTENTION